Project no.: **335091**

TIDE

Scientific and Technical Results

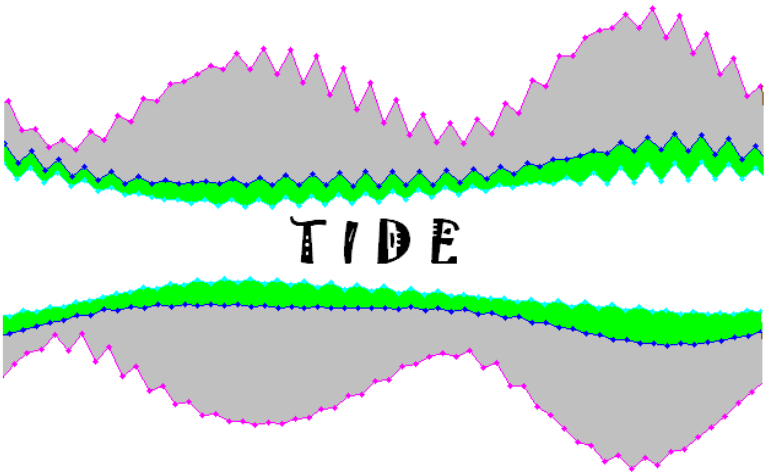

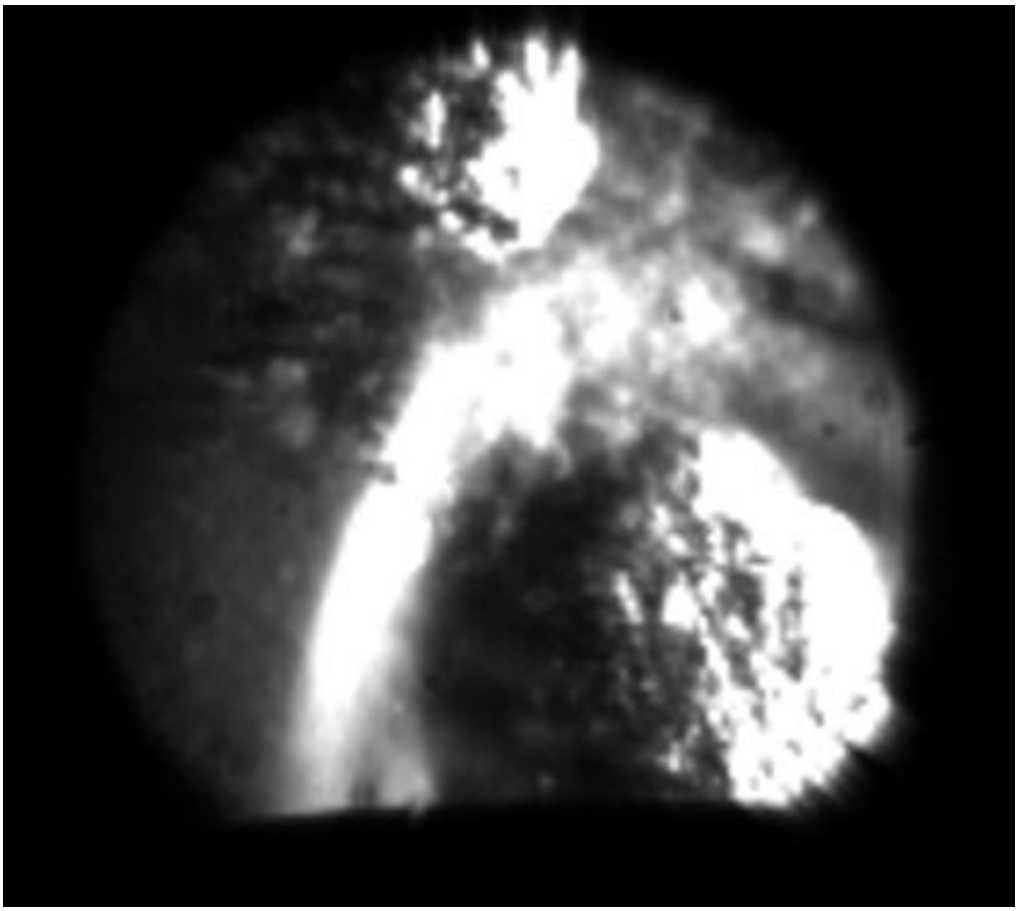

1. Main scientific and technical results

1.1. WP 2 – Preliminary concept design

The most important result obtained in this WP was the development of a methodology for calculating the thermodynamic cycle of the engine.

The thermodynamic cycle of the engine is comprised of the specific processes for each major component: real compression in the compressor, detonation in the PDC, and real expansion in the PDC channel and exhaust nozzle. The equations used to model these thermodynamic evolutions in terms of pressure, specific volume, temperature, enthalpy and entropy will be presented in the following paragraphs.

Significant results were obtained for modelling the detonation process, which was carried out using two approaches. In the first, Zeldovich – von Neumann – Doring (ZND) thermodynamic cycle was used. In the second, the NASA – Glenn Chemical Equilibrium Program CEA2 was employed to determine another set of thermodynamic properties.

By applying the above two models, the results presented in Table 1 and in Figure 1 were obtained for the operating conditions of the TIDE engine. A reference Brayton cycle operating under the same initial conditions was added for reference purposes.

The net work, the cycle efficiency and the power are provided in Table 2.

Table 1 – Thermodynamic cycle results

St.	p [Pa]	T [K]	v [m^3 / kg]	s [J/kg K]
1	110330	288.00	0.81656	6660.122
2	607980	528.17	0.24959	6755.181
ZND				
$3'_Z$	2075256	1589.65	0.22007	7510.422
3_Z	1190576.2	2859.19	0.60311	8664.578
4_Z	101330	2067.63	5.12440	8723.095
CEA				
3_C	3438399.6	3281.64	0.23969	10971.500
4_C	101330	2071.72	5.13450	11061.584
Brayton				
3_B	607980	2354.64	1.08376	9264.811
4_B	101330	1795.39	4.95815	9310.917

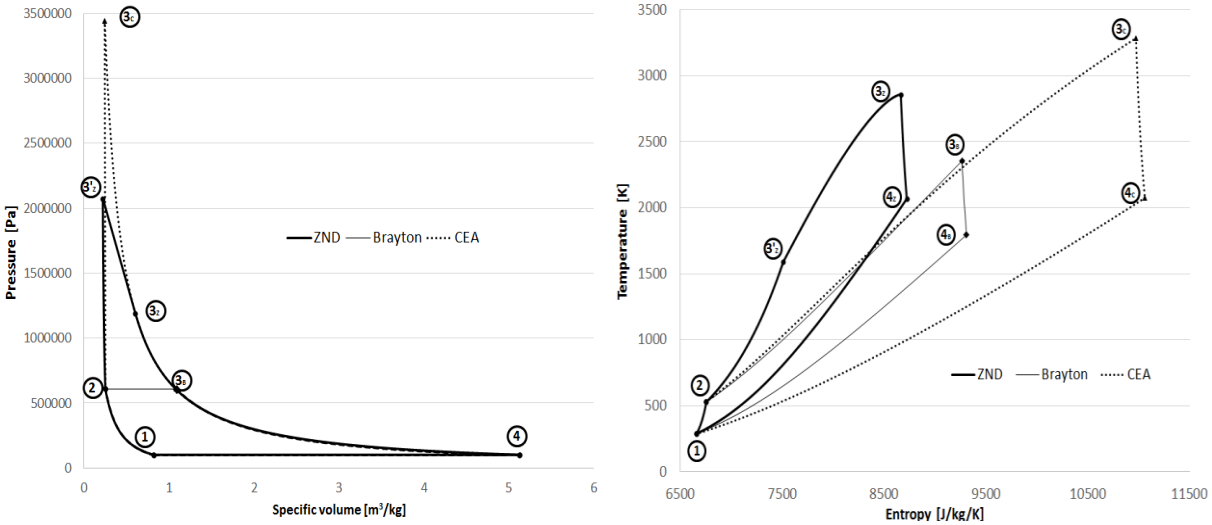

Figure 1 – p-v (left) and T – s (right) diagram of the real TIDE cycles

© TIDE Consortium - *This document and the information contained are TIDE consortium property and shall not be copied or disclosed to any third party without TIDE consortium prior written authorisation*

Table 2 – Net work, cycle efficiency and power

Cycle	Net specific work [J/kg]	Cycle efficiency [%]	Cycle averaged power [kW[
ZND	1330833	38.89	1668.9
CEA	1431103	41.82	1794.6
Brayton	828688	24.21	828.7

1.2. WP 3 – Numerical simulations

Key results have been achieved in the numerical simulation for the compressor, combustor, and the entire engine.

The compressor calculations were initialized by specifying the lower static pressure at compressor outlet. These results were used for starting the compressor flow numerical simulation using the design-point outlet mass flow rate of 1.70 kg/s. After about 1500 iterations, the steady calculation converged, the residuals of the RANS equations and of the two turbulent equations decreasing by at least two orders of magnitude. The dimensionless imbalance of inlet and outlet mass flow rate was around 2.4 x 10^{-5}. The compressor design-point overall aerodynamic performance and the corresponding mass-averaged flow quantities at compressor inlet and outlet are listed in Tables 3 and 4 respectively.

Table 3 – The design-point overall aerodynamic performance

Quantity	Unit	Value
Mass Flow Rate	kg/s	1.70 [kg/s]
Input Power	W	722483.00 [W]
Inlet Flow Coefficient	-	2.94 x 10^{-2}
Exit Flow Coefficient	-	9.87 x 10^{-2}
Head Coefficient	-	3.59
Work Input Coefficient	-	0.72
Static-to-total Pressure Ratio	-	6.76
Total-to-total Pressure Ratio	-	14.23
Total-to-total Temperature Ratio	-	2.41
Total-to-total Isentropic Efficiency	-	80.57%
Total-to-total Polytropic Efficiency	-	86.28%

Table 4 – The mass-averaged flow quantities at compressor inlet and outlet

Quantity	Unit	Inlet	Outlet
Static pressure	[Pa]	90126.60	684691.00
Total pressure	[Pa]	101313.00	1442040.00
Static temperature	[K]	290.16	584.64
Total temperature	[K]	300.03	723.20
Static enthalpy	[J/ kg]	-8023.61	287749.0000
Total enthalpy	[J/ kg]	1889.23	426921.00
Entropy	[J / kg K]	6.35	127.95
Absolute Mach number	-	0.41	1.08
Relative Mach (number	-	0.99	0.62

For the unrecovered kinetic energy of flow leaving the impeller exit, a backsweep blade design was used to reduce the net circumferential speed and to decreases the effective through-flow area at the rear part of compressor impeller resulting in a local acceleration of the relative subsonic flow in the rotating frame. In the present case, the unrecovered kinetic energy even contributes to more than half the amount of the total-to-total pressure ratio (14.23:1) against the static pressure rise.

Considering there is no diffuser in the compressor, the kinetic energy of flow leaving the impeller exit can`t be recovered to static pressure rise. So the static-to-total pressure ratio is more realistic rather than

© TIDE Consortium - *This document and the information contained are TIDE consortium property and shall not be copied or disclosed to any third party without TIDE consortium prior written authorisation*

the total-to-total pressure ratio. With the specified outlet mass flow rate of 1.70 kg/s, the calculated static-to-total pressure ratio is 6.76. Compared with the baseline static-to-total pressure ratio of 6.00, the present case gets extra 0.76 bar static pressure rise. This provides compensation for the possible under-estimated pressure loss generated before impeller exit flow arrives at the combustor inlet, and in other words can better match the compressor with the succeeding combustor.

The backsweep blade design also lowers the flow turning resulting in a decrease of blade loading, contributing to the suppression of the unfavourable recirculation zones that may form inside the rear part of impeller passage. This results in a total-to-total isentropic efficiency of 80.57%.

Several regions of high impact on the compressor performances were analyzed in detail:

Leading edge flow

Figures 2 – 4 show the blade-to-blade distribution of the relative Mach number and the relative velocity field at 20%, 50% and 80% of the span from the hub, respectively. The relative inlet flow meets the leading edge of the main blade, and rapidly accelerates along the suction surface. The inlet incidence angle is very small in general. Higher inlet incidence angle only exists near the hub, and leads to the secondary flow, shown in Figure 5a. The peak Mach number of the accelerating flow near the suction surface is around 1.0 along the span (except near the hub), as shown in Figure 5b. This transonic flow is followed by shock wave, which, especially above 50% span is strong and nearly normal to the suction surface. Its interaction with the boundary layer further stimulates the development of the latter.

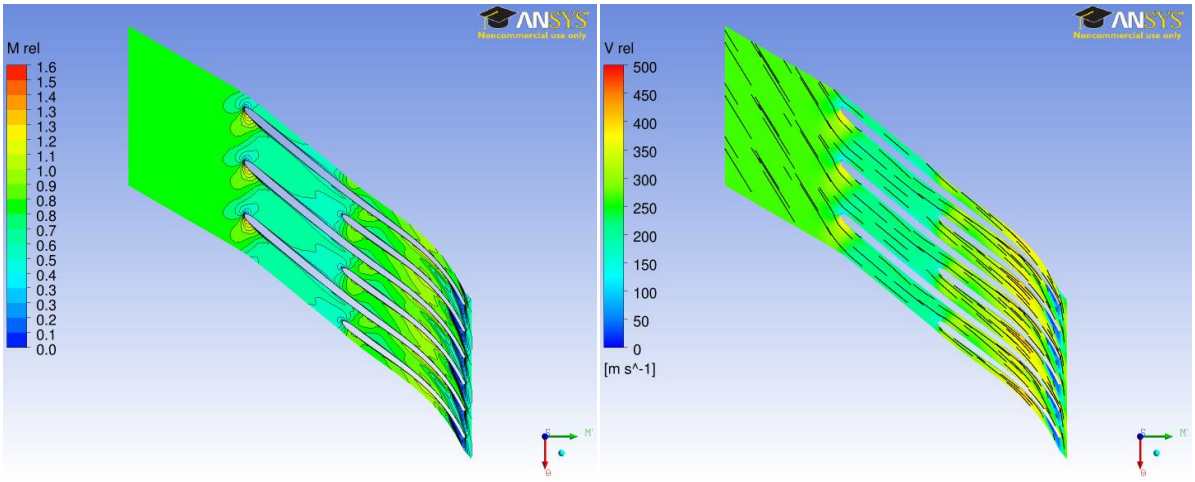

(a) (b)

Figure 2 – The blade-to-blade distribution of relative Mach (a) and relative velocity (b) at 20% span

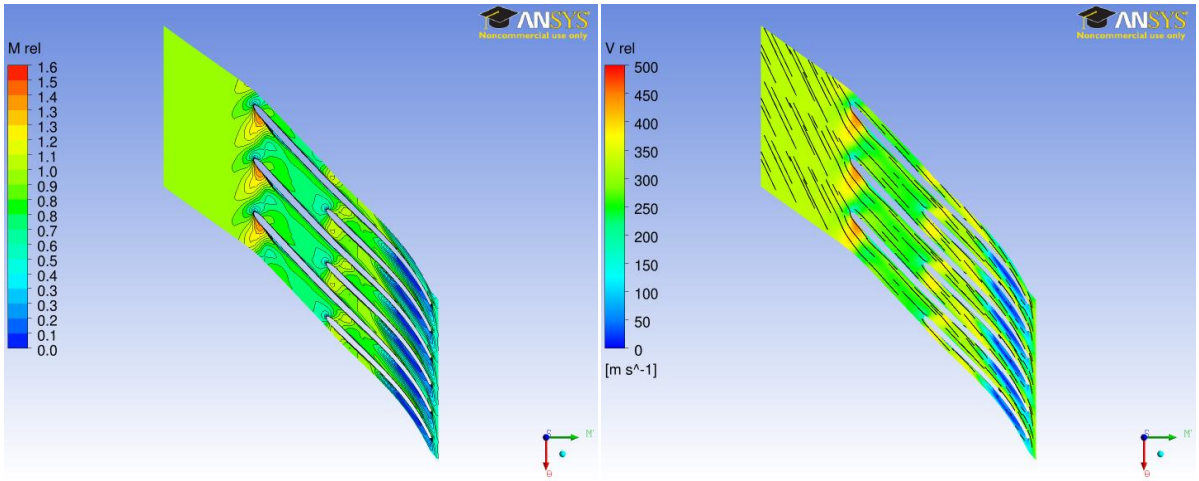

(a) (b)

Figure 3 – The blade-to-blade distribution of relative Mach (a) and relative velocity (b) at 50% span

© TIDE Consortium - *This document and the information contained are TIDE consortium property and shall not be copied or disclosed to any third party without TIDE consortium prior written authorisation*

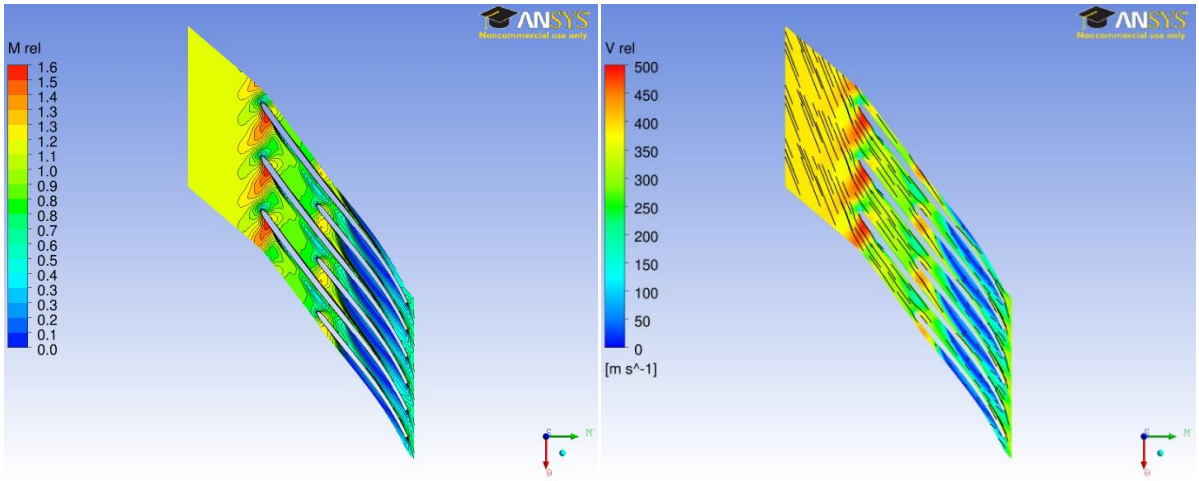

(a) (b)

Figure 4 – The blade-to-blade distribution of relative Mach (a) and relative velocity (b) at 80% span

The low-momentum and non-isentropic flow region induced by the shock wave and boundary layer interaction can be observed after the shock wave near the suction surface. At the front part of the main blade after the shock wave, the airfoil loading at 80% span is slightly higher than that at 20% and 50% span, as shown in Figure 6, exaggerating the low-momentum region transported downstream towards the leading edge of the splitter blade.

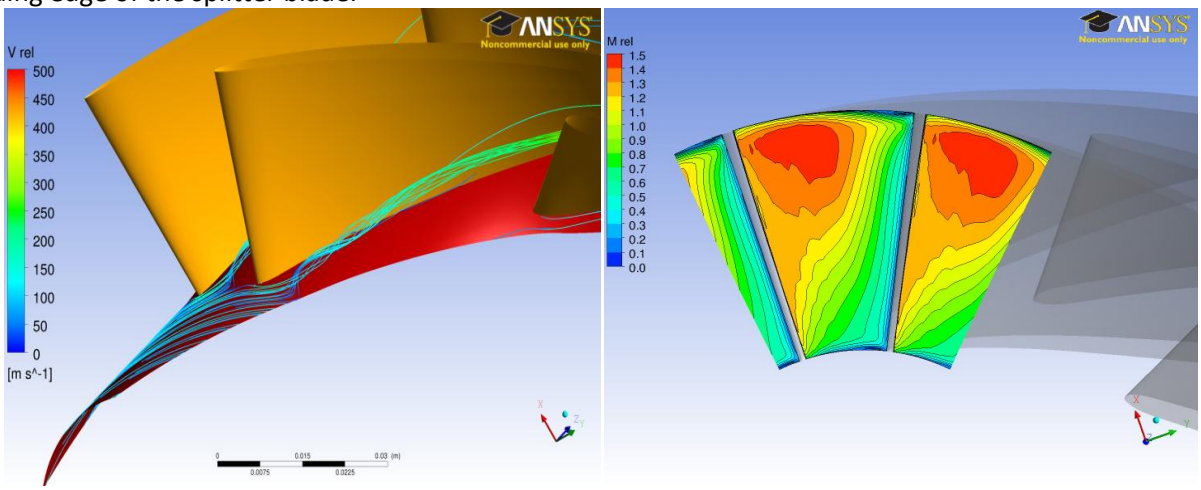

(a) (b)

Figure 5 – The tracer of secondary flow from the hub (a) and the contour of relative Mach number at leading edge of the main blade (b)

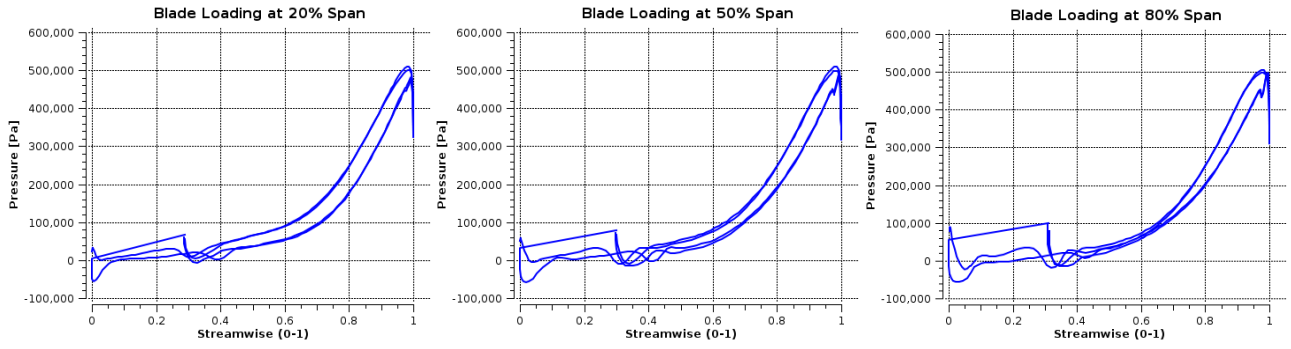

(a) (b) (c)

Figure 6 – The blade loading at 20%, 50% and 80% span

© TIDE Consortium - *This document and the information contained are TIDE consortium property and shall not be copied or disclosed to any third party without TIDE consortium prior written authorisation*

Oppositely, the low momentum region at 20% and 50% span is closed to the wall and vanishes over a short distance. The entropy distribution, shown in Figure 7) is a good tracer for the downstream migration of the low momentum flow, indicating that main loss between the leading edge of main blade and the leading edge of splitter blade is the shock loss and the induced separation loss at 80% span.

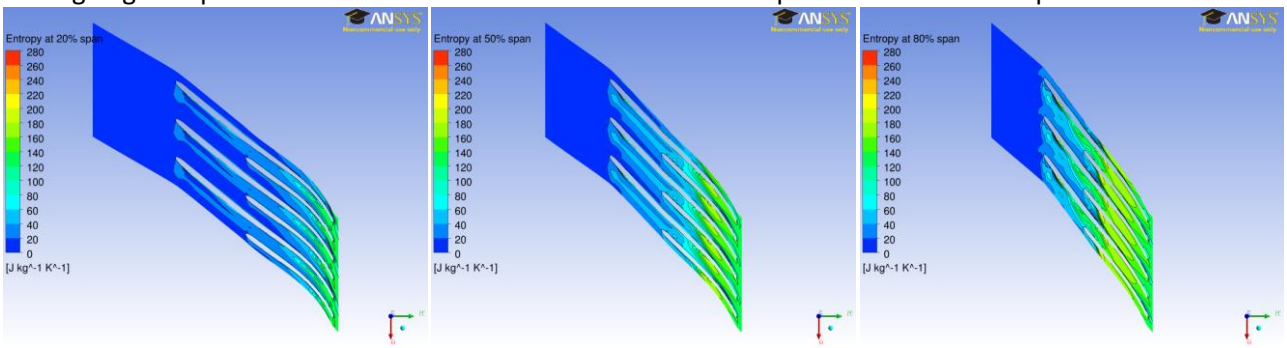

(a) (b) (c)

Figure 7 – The blade-to-blade distribution of entropy at 20%, 50% and 80% span

Before arriving at the leading edge of the splitter blade, due to the relative low-level cross-section pressure gradient compared with that at the aft part of the impeller shown in Figure 5b, the overall development of the secondary flow is slow, making the flow generally less non-uniform.

This provides very good inlet flow condition for the splitter. And also the velocity vector fields in Figures 2 – 4 shows that along the whole span the flow angle is in good match with the airfoil mean line angle at the leading edge of the splitter blade. The arrangement of low blade loading distributed in the front part of the impeller relieves the development of the secondary flow.

Recirculation zone

In the front part of the impeller, the lower blade loading distribution provides a good inlet condition for the splitter blade. The splitter blade separates the upstream homogenous flow into two branches. Because the impeller is enclosed, there is no tip clearance flow across the two branches. The flow entering these two branches joins together at the impeller exit.

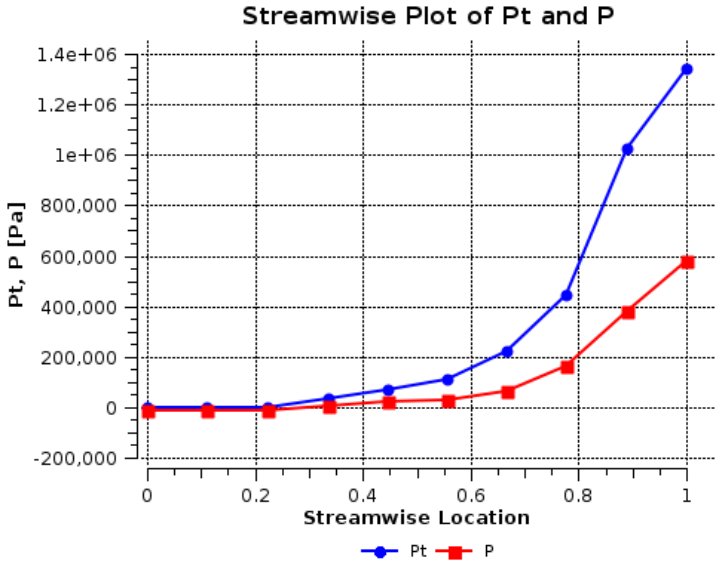

Figure 8 – The streamwise distribution of the mass-average static and total pressure

Apart from the blade loading existing at the leading edge of the main blade, most of the loading is distributed at the aft part of the impeller shown in Figure 6. Figure 8 shows that the mass-averaged static and total pressure rise is achieved mainly by the blade loading at the aft part of the impeller and high

© TIDE Consortium - *This document and the information contained are TIDE consortium property and shall not be copied or disclosed to any third party without TIDE consortium prior written authorisation*

centrifugal force. This kind of blade loading distribution and pressure rise characterizes an aft-loading airfoil. The secondary flow develops quickly in the aft part and creates a flow velocity difference in the across section. Even if the smaller loading near the shroud can reduce the velocity difference in the cross section near the shroud, the formation of the low momentum non-isentropic recirculation zones balances this velocity difference triggered by the blade loading with the help of the shroud curvature radius.

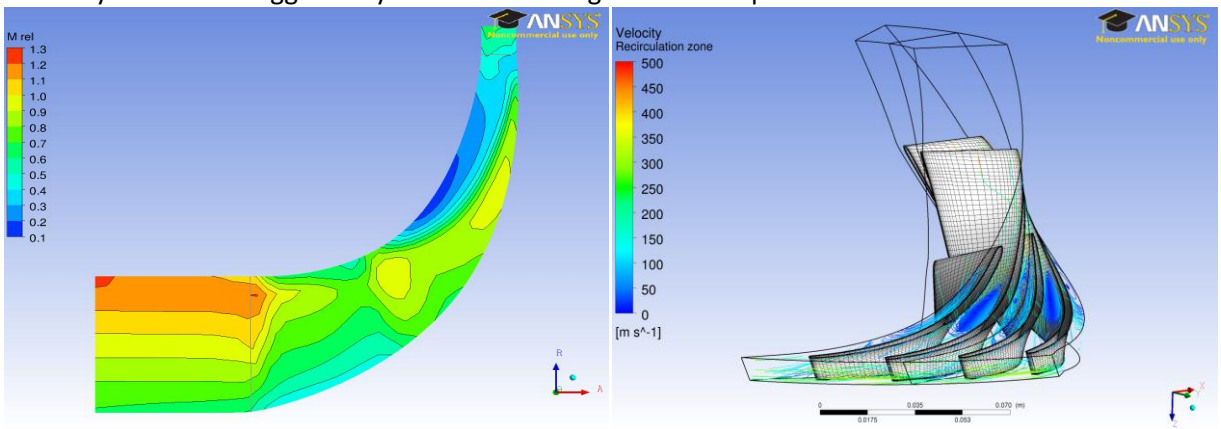

Figure 9 – The contour of mass averaged relative Mach number on meridional surface (left) and the 3D view of the recirculation zone (right)

Figure 9 shows the development of the recirculation zone. Its onset is from the corner bounded by shroud and blade suction surface. Because the cross-section area of the meridional path is shrunk along the streamwise direction from inlet to outlet, the recirculation flow holds a large amount area of the cross section in the downstream development, making the high-speed isentropic flow turning toward to the blade pressure surface, shown in Figures 2 – 4, and toward to the hub, shown in Figure 9 (left). In the succeeding, part of the recirculation flow is reattached near the shroud, while the other part is transported to the hub resulting flow separation between hub and blade suction surface. Thus the flow is fully three-dimensional and turbulent. After the reattached zone near shroud, the flow again accelerates until the compressor outlet, and the flow angle is agreed well with the blade mean line angle shown in Figure 4. At the trailing edge near hub, when the jet flow from the pressure side meets the separation flow from the suction surface, the flow angle deviated from the blade meanline angle apparently.

The advantage of the backsweep angle design is apparent with respect to the recirculation zones at the aft part of the impeller, which tend to resist the centrifugal force and affect the compressor performance, e.g. the head rise and power consumption. Compared with the straight radial blade, the airfoil loading of the backsweep blade is reduced due to the under-turning flow and the flow velocity difference at the cross section is also lowered. Before the flow leaves the impeller exit, the two recirculation zones are nearly stabilized and localized without large amount low-momentum flow out of the impeller exit.

Concluding, the compressor numerical simulations resulted in the following main findings:

- The flow angle at the inlet of impeller in general agrees well with the blade mean line angle except the hub. The interaction of shock wave and boundary layer near shroud triggers small flow separation.
- The impeller blade is an aft-loading airfoil. The lower loading at the front part of the impeller makes the inlet flow less non-uniform. At the aft part of the impeller, the airfoil loading together with the curvature radius of shroud forms recirculation zones.
- The high backsweep angle and zero inclination of impeller leading edge partly release the airfoil loading and successfully suppress the recirculation zone. This essentially insures that the designed centrifugal compressor achieves the requirements of the TIDE engine.

The combustor numerical simulations consisted of non – reactive and reactive numerical simulations. The non – reactive simulations were carried out to verify that supersonic flow is achieved inside the combustor, to analyze the correlation between the pressure waves travelling in the main combustion chamber and in the resonators, and to verify the temperature at the back wall of the main combustion

© TIDE Consortium - *This document and the information contained are TIDE consortium property and shall not be copied or disclosed to any third party without TIDE consortium prior written authorisation*

chamber. It was found that the air accelerates to supersonic velocities in the divergent nozzle downstream of the critical section. The frequencies of the pressure signals in the two lateral resonators and in the central detonation chamber are equal, of about 3250 Hz, but the oscillations are of opposite phase (pressure maxima in the resonator correspond to pressure minima in the main combustion chamber). The amplitude of the pressure oscillations is higher in the resonator than in the main combustor, and it slowly decreases in time for both considered regions. The instantaneous temperature field was observed to exceed locally the Hydrogen auto-ignition temperature.

The combustor reactive flow numerical simulation showed that the detonation cycle can be divided into four phases: the ignition phase, the detonation propagation phase, the flow cooling phase, and the readmission phase.

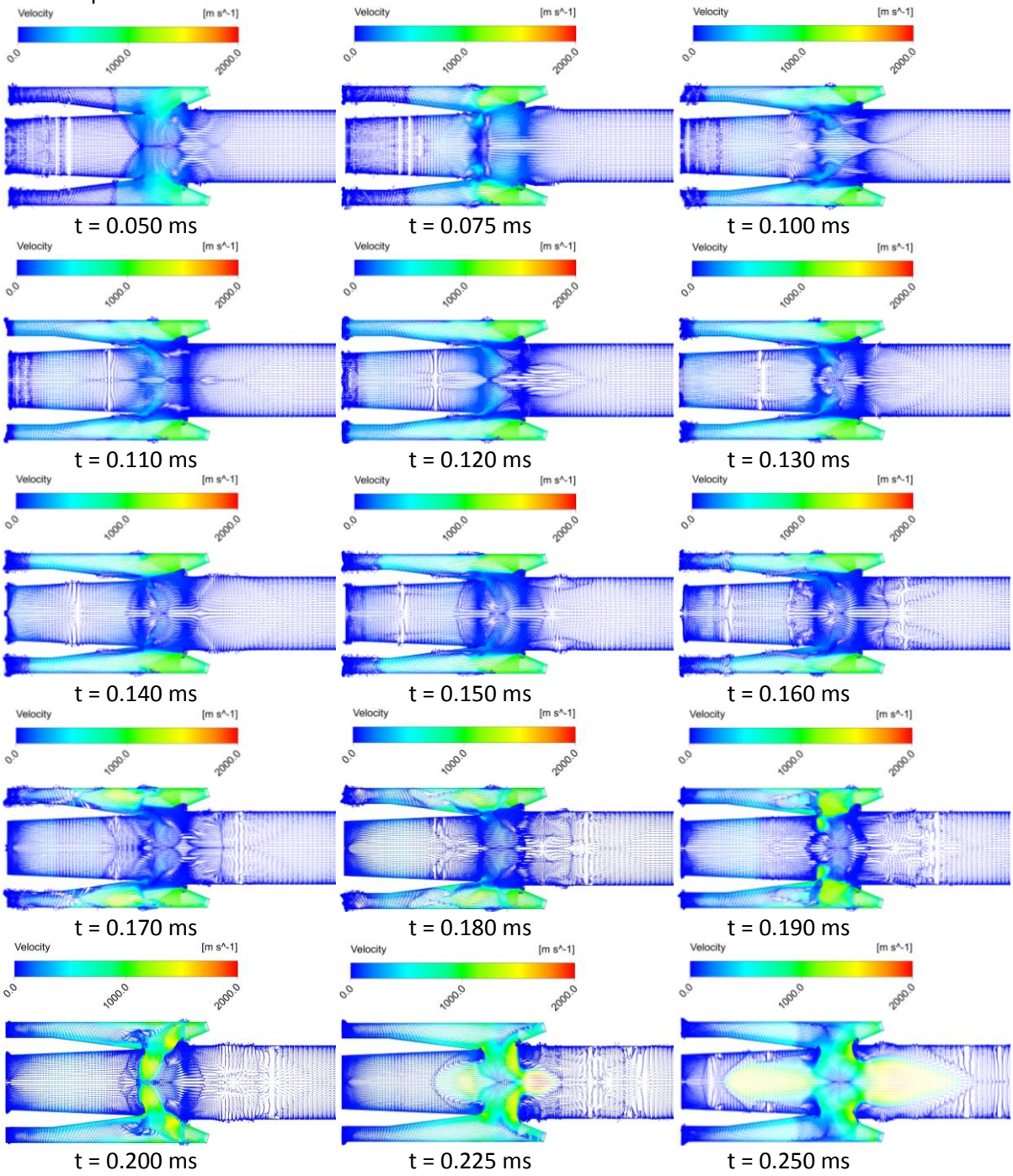

Figure 10 – Instantaneous velocity vector fields between 0.05 ms and 0.25 ms, coloured by magnitude

© TIDE Consortium - *This document and the information contained are TIDE consortium property and shall not be copied or disclosed to any third party without TIDE consortium prior written authorisation*

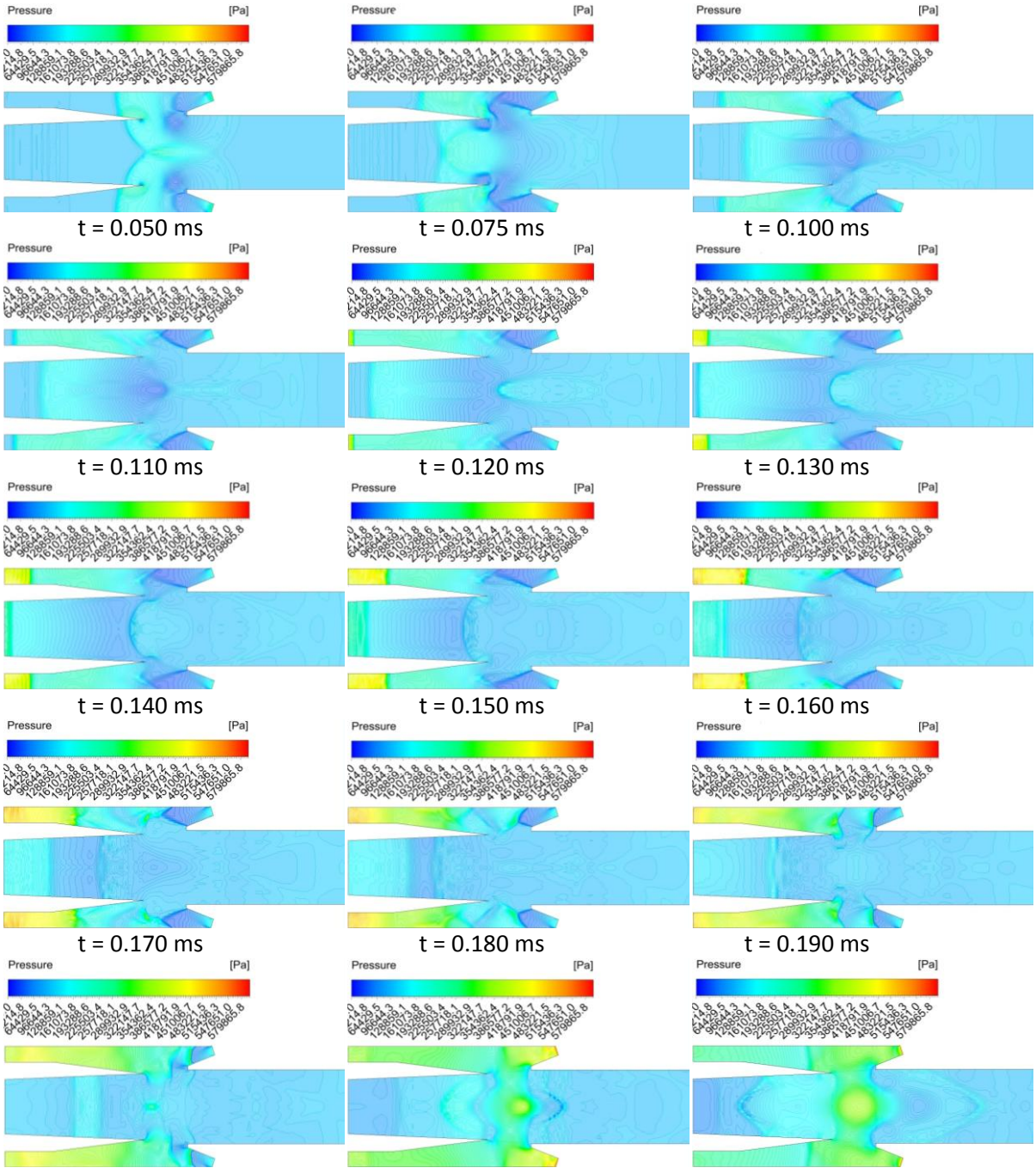

Figure 11 – Instantaneous pressure scalar fields between 0.05 ms and 0.25 ms

During the ignition phase, the numerical simulation shows that self – ignition of the stoechiometric fuel – air mixture occurs at 0.150 ms after the flow starts to flow into the PDC, in two symmetrical positions inside the lateral resonators, in the straight channel at the middle of their vertical dimension and around the middle of the straight channels of the resonators, in the axial direction.

The flow enters the PDC with a slightly higher temperature (500 K) than the atmospheric air initially filling the PDC. A bow expansion wave appears at the supersonic nozzle exit.

The air stream resulting from the two supersonic jets first enter the two lateral resonators where they create pressure waves propagating axially along the flow direction both in the lateral resonators, but also into the central detonation chamber.

© TIDE Consortium - *This document and the information contained are TIDE consortium property and shall not be copied or disclosed to any third party without TIDE consortium prior written authorisation*

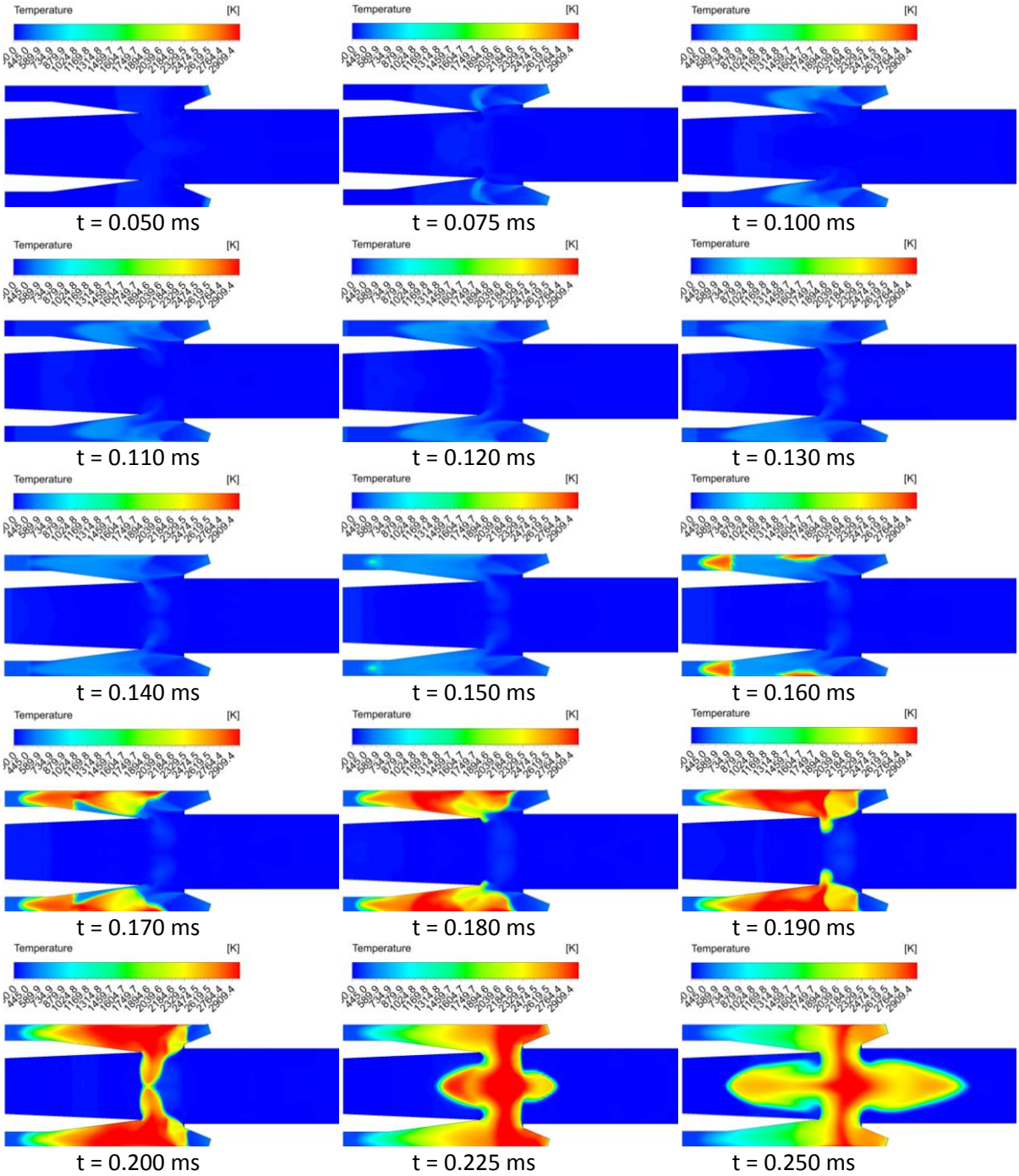

Figure 12 – Instantaneous temperature scalar fields between 0.05 ms and 0.25 ms

As the high speed jets flow into the resonators, flow is entrained from the stagnant central detonation chamber into the lateral resonators, increasing the pressure levels there, and the intensity of the pressure waves propagating inside the lateral resonators. The entrained air interferes with the incoming jets composed of premixed Hydrogen and air and creates vortices that pushed the combustible mixture into the central detonation chamber. The mixture in this region is then slowly convected in both axial and transversal direction by the low velocity flow existing here, and will play a critical role in the transition from deflagration to detonation.

The pressure waves mentioned earlier reach the solid back wall of the lateral resonators and the pressure in the region close to the closed ends of the lateral resonators starts rising sharply. The pressure waves are reflected back by the back wall of the lateral resonator and start moving towards the incoming

© TIDE Consortium - *This document and the information contained are TIDE consortium property and shall not be copied or disclosed to any third party without TIDE consortium prior written authorisation*

supersonic jets, which are still flowing towards the closed ends of the resonators. The flow behind the pressure waves reverses direction entrained by the pressure gradient.

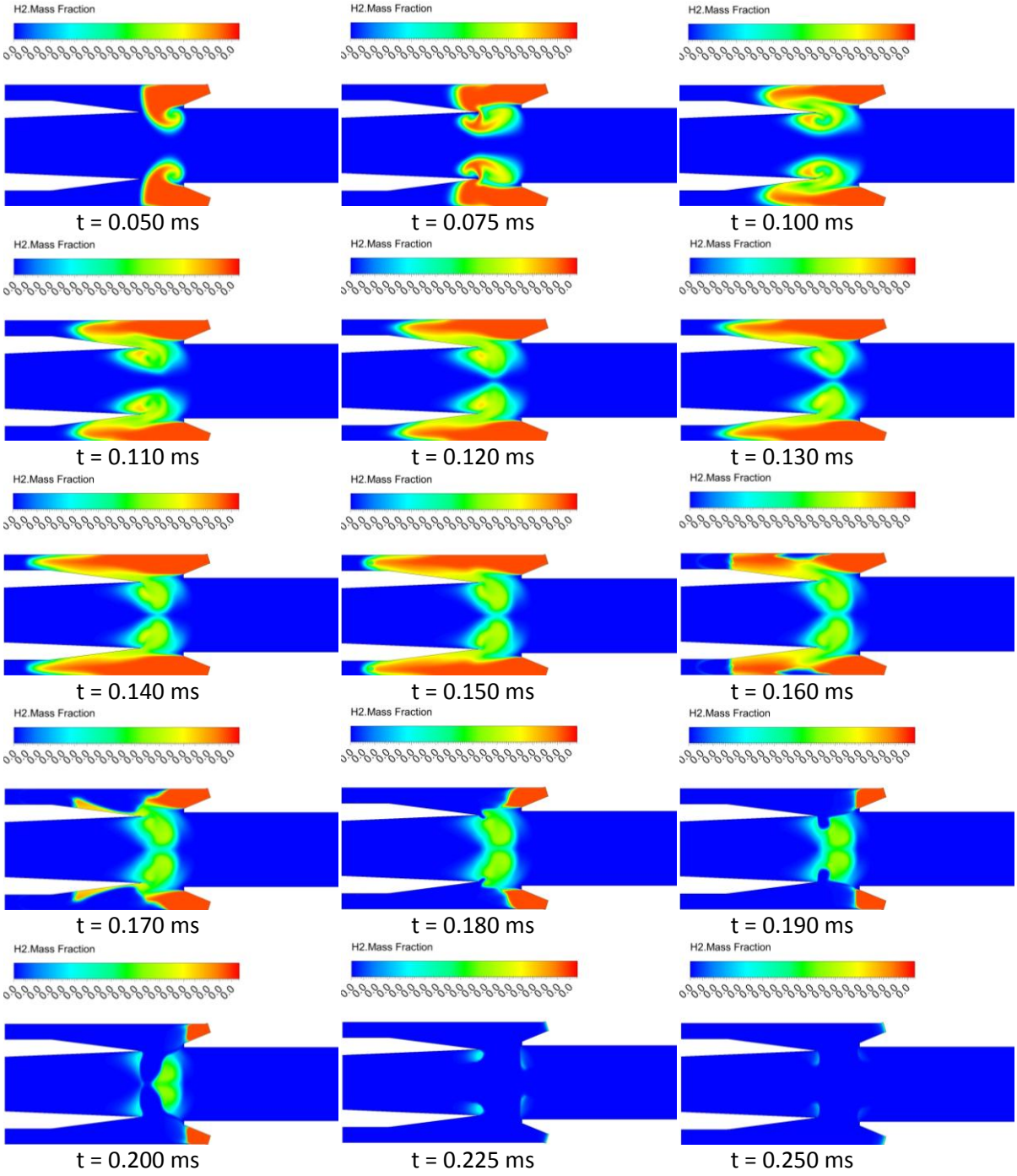

Figure 13 – Instantaneous Hydrogen mass fraction scalar fields between 0.05 ms and 0.25 ms

When the pressure waves returning from the back wall and meet the incoming jets, the local pressure increases even higher and forces the flow in the supersonic jets to break suddenly, triggering the formation of a shock wave around the middle of the straight channel of the lateral resonator. At this point, the temperature rises sharply through the shock wave due to the meeting of the two sudden breaking of the air streams, and the fuel – air mixture starts propagating upstream, as a deflagration wave, through the fresh mixture in the supersonic jets.

© TIDE Consortium - *This document and the information contained are TIDE consortium property and shall not be copied or disclosed to any third party without TIDE consortium prior written authorisation*

The combustion process spreads through the lateral resonators until they are almost completely filled with combustion products. Meanwhile, the shock waves propagate upstream through the lateral resonators increasing the local pressure, and forming typical shock cell structures.

The increasing pressure starts flattening the bow expansion wave formed at the exhaust of the two nozzles, while also pushing it back, inside the supersonic nozzles.

The local pressure in the lateral resonators regions, close to the PDC lateral walls, increases, and the direction of the incoming supersonic jets is deflected towards the central region of the PDC.

The flow in the lateral resonator reverses direction, now towards the supersonic nozzles. At this time, the flame reaches the central region of the PDC, and starts propagating mainly in the transversal direction through the combustible mixture brought here by the entrainment vortices mentioned earlier. The sudden increase in temperature in the central detonation chamber inlet triggers a sudden increase in pressure in the central region of the PDC. The pressure gradient occurring between this region and the neighbouring zones, both upstream and downstream creates a strong acceleration in the axial direction, up to supersonic values. The incoming supersonic jets suffer a sharp turn immediately after exiting the nozzles, and the flow pattern becomes similar to the non – reactive case flow, presented in the previous section. A central supersonic jet oriented towards the outlet of the PDC is formed, delimited by a strong shock wave also propagating outwards. The combustion front is coupled and rides right behind this travelling shock wave, in a typical detonation front pattern.

The pressure in the supersonic nozzle is higher now than the inlet pressure, and the flow of fresh mixture into the PDC is blocked.

Details on the evolution of the velocity vector field and scalar pressure, temperature, and fuel mass fractions during this phase are provided in Figures 10 – 13.

Once the detonation is initiated in the central region around t = 0.225, the detonation propagation phase starts, towards the PDC exit. The velocity in the central jet core increases as long as it is supported by combustion, mainly in the axial direction. The direction of the supersonic jets remains largely unchanged during this phase, with a sharp turning of the jets immediately downstream of the exits of the supersonic nozzles, due to the large pressure in the region between the nozzles exits and the entrance in the two lateral resonators.

In the central jet region, the pressure gradually decreases as the combustion process stops due to the depletion of fuel. The pressure wave propagating towards the back wall of the central detonation chamber reaches the wall and is reflected backwards, while the pressure behind it decreases due to the increasing volume available. Due to the combined effect of disappearing combustion and expansion behind the reflected wave, the pressure in the central detonation chambers tends towards a uniform value.

In the lateral resonators and at the exit of the two supersonic nozzles, the pressure levels remain high enough to stop the admission of the combustible mixture into the PDC.

However, the temperature inside the supersonic nozzle remains in the numerical simulation carried out at this task high enough continue to ignite the fresh mixture whenever the pressure in the divergent section of the nozzle decreases enough to allow it to enter the computational domain.

This effect is an artefact of the numerical simulation, in contradiction with the experimental observations to be presented later. Several reasons may be responsible for the numerical simulation not capturing the actual behaviour of the flow inside the PDC. First, the combustion model used for the numerical simulation (EDM) is known to over predict the flame thickness in reactive flow simulations. As a result, the flame is less responsive to flow gradients, particular velocity gradients creating stresses and strains, and is much harder to quench. Also, the boundary condition imposed on the PDC solid walls were specific to adiabatic walls, preventing the normal loss of heat through the wall to the environment and artificially supporting a high temperature being maintained inside the supersonic nozzles.

Finally, the computational domain is limited to the critical section of the Laval nozzles, thus preventing pressure waves to travel upstream into the subsonic region of the nozzles, and to create full flow reversal through the nozzles. This way, the fresh mixture is always ready to enter the diverging part of the nozzle supporting combustion and not allowing the proper cooling of the flow inside the nozzles.

© TIDE Consortium - *This document and the information contained are TIDE consortium property and shall not be copied or disclosed to any third party without TIDE consortium prior written authorisation*

To circumvent this shortcoming of the numerical simulation, the flow through the two supersonic nozzles was artificially stopped by closed the computational domain inlets placed in the critical sections of the nozzles.

A new phase, the flow cooling phase, started at this point, and the numerical simulation in this phase used a zero velocity boundary condition at the inlet. All the other boundary conditions remained unchanged.

The effect of closing the inlet nozzles is immediately visible in the velocity fields. The tangential velocity components decrease suddenly once the incoming supersonic jets disappear, and remain at very low values throughout the current phase. The axial velocity approaches zero almost immediately after the inlets are closed. The central jet velocity decreases much slower, supersonic velocities being maintained for a significant amount of time. The central detonation chamber velocity also decreases, at about the same pace. As the jets disappear, the flow angle with respect to the PDC centreline in the central region decreases gradually.

The temperature starts also decreasing throughout the PDC, with high temperature regions being maintained towards the outlet, where the influence of the hot central jet core is still present, and near the PDC walls, particularly in the central detonation chamber and in the divergent parts of the two supersonic nozzles.

The lateral resonators cool much faster, since their temperature was much lower at the beginning of the phase anyway.

The water mass fraction field evolves in a pattern very similar to the temperature. Since, in the absence of combustion, no more water is produced, the water accumulated in the central detonation chamber and, partially, in the divergent section of the two nozzles is convected away, towards the exhaust of the PDC.

The admission of fresh mixture in the computational domain is obviously blocked.

The pressure starts decreasing first in the middle of the region placed between the central jet core and the back wall, both in the central detonation chamber and in the lateral resonators. The pressure waves are reaching the PDC back wall and are reflected back towards the PDC outlet, while the general pressure level inside the PDC continues to decrease towards the atmospheric level.

Once the temperature immediately downstream of the critical sections of the two convergent – divergent nozzles dropped below the self – ignition point for Hydrogen, the initial simulation boundary conditions were reinstated, and fresh mixture was again admitted into the computational domain initiating the readmission phase. Obviously, fresh mixture enters the divergent region of the two supersonic nozzles and is convected into the PDC. The colder fresh mixture decreases the temperature in the nozzles below the ignition point of the fuel, and no combustion products are formed in the nozzles.

The pressure rises into the nozzles again and creates pressure waves that start propagating mainly into the two lateral resonators, restarting the detonation cycle. As before, the direction of the supersonic jets exiting the nozzles is towards the lateral resonators. From this point, the flow patterns inside the PDC are repeating the previous cycle, with a new ignition phase, followed by the detonation propagation phase, and the cooling phase.

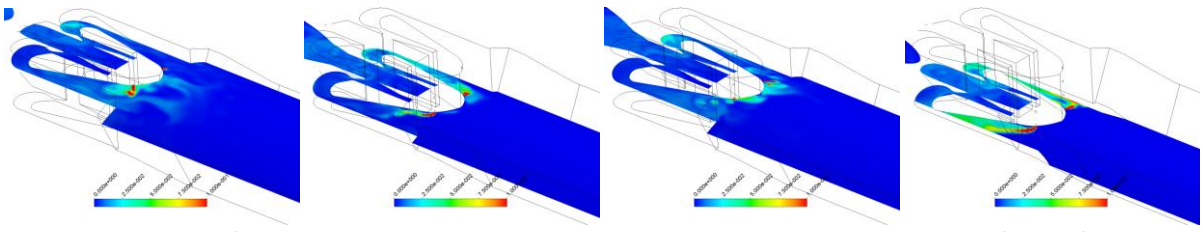

Figure 14 – Fuel mass fraction at 4 radial planes corresponding to the centre position of each fuel inlet pair

The numerical simulation of the whole TIDE engine could not capture the detonation process. Non-reactive numerical simulations were carried out in order to assess the aerodynamic performance of the engine and to verify the overall engine design. Figure 14 shows the instantaneous mass concentration of

© TIDE Consortium - *This document and the information contained are TIDE consortium property and shall not be copied or disclosed to any third party without TIDE consortium prior written authorisation*

fuel at four radial planes corresponding to the centre of each fuel inlet. At the lowest radial position one can clearly observe jet-in cross-flow behaviour of the fuel injection.

The fuel jet is bent in the flow direction and the fuel is convected downstream fairly symmetrically. As the resonator is reached the fuel air mixture is reasonably homogeneous. However, already at the next pair of injectors the one can observe a strong difference between the fuel distributions at the two sides. This is most probably due to the strong rotation of the engine. The rotational motion of the engine is from right to left in the picture. Hence, the left side fuel injectors will henceforth be called leading side injectors and right ones trailing side injectors. As can be observed at the second lowest injector pair the concentration on the trailing side is much larger then on the leading side. This difference is even more pronounced at the two upper injection positions. At these position a second phenomenon also appears, namely a back flow of fuel into the plenum. This becomes stronger as the radius increases. Again the effect of the strong rotation in combination with the almost stagnant flow in the plenum is the most probable cause.

For further insight into the fuel transport we consider planes at several axial positions from the fuel inlet and downstream as is outlined in Figure 15. At the fuel inlet one can clearly see the jets issuing into the main air flow. It is worth noticing that at the two lower positions the jets are directed slightly downwards. At all the downstream positions a strong concentration gradient in the radial direction is observed. Much of the fuel accumulates at the inner radius and there is also a distinct difference between the leading and trailing channel channels. Regarding the concentration inside the resonator the leading-trailing difference is also visible here as well as the radial concentration gradient. It is not until the flow reaches the entrance to the nozzle one sees a relatively homogeneous air-fuel mixture. There is some fuel present in the resonator part but mainly located towards the inner radius.

In Figure 14 it was noted that at the upper fuel inlets there was some back flow of fuel. Now considering two radial planes upstream of the fuel inlets we see that this is indeed the case. Close to the outer radius we get an accumulation of fuel even as far as 6 cm upstream of the fuel inlets as can be seen in Figure 16. Figure 17 shows the temperature at the same positions as concentration in Figure 14. A similar radial variation as for pressure in the previous report is seen. Close to the inner radius the temperature is about 650 K and at the outer it is about 850 K. This difference originates from the plenum, as is seen in Figure 18 and persists all through the combustor.

The asymmetry in the fuel distribution shown above might be explained by considering the flow field at some positions. Figure 18 shows the flow field at the radial plane through the upper fuel inlets. There is a tendency for some back flow on the border between combustor and plenum and also some flow in the tangential direction against the direction of rotation.

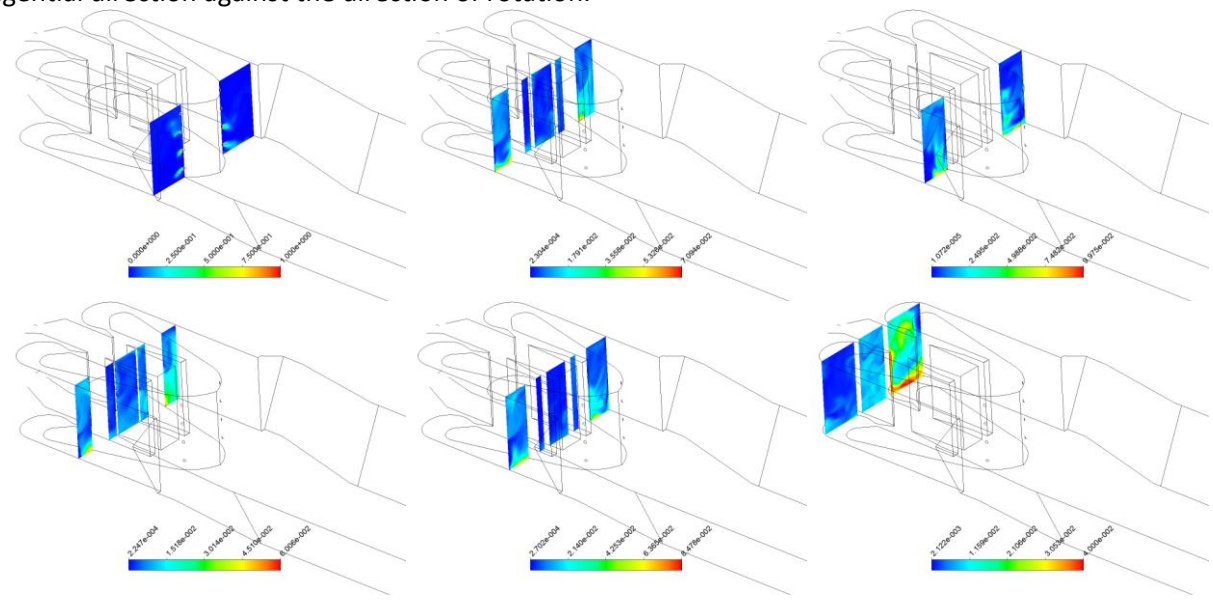

Figure 15 – Fuel mass fraction at 6 axial positions from the fuel inlets and downstream

© TIDE Consortium - *This document and the information contained are TIDE consortium property and shall not be copied or disclosed to any third party without TIDE consortium prior written authorisation*

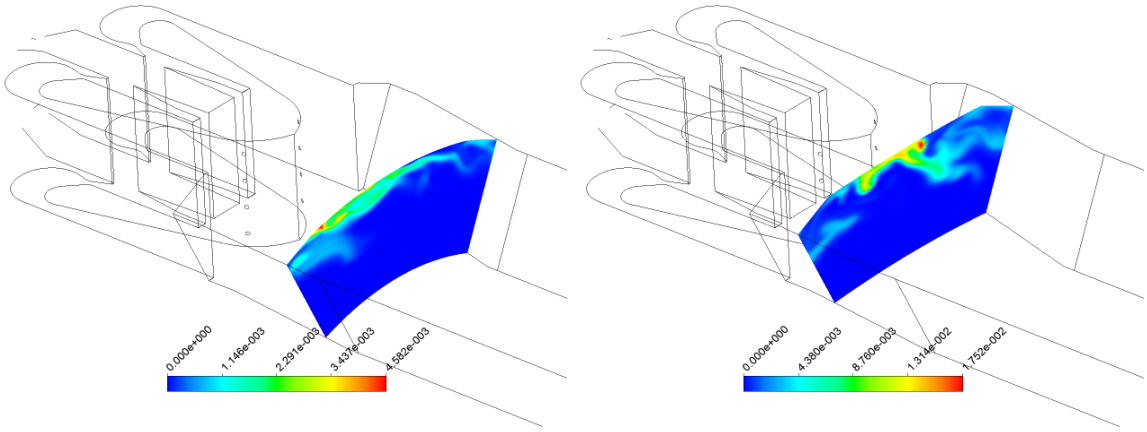

Figure 16 – Fuel mass fraction at 3 (right) and 6 cm upstream of the fuel inlets

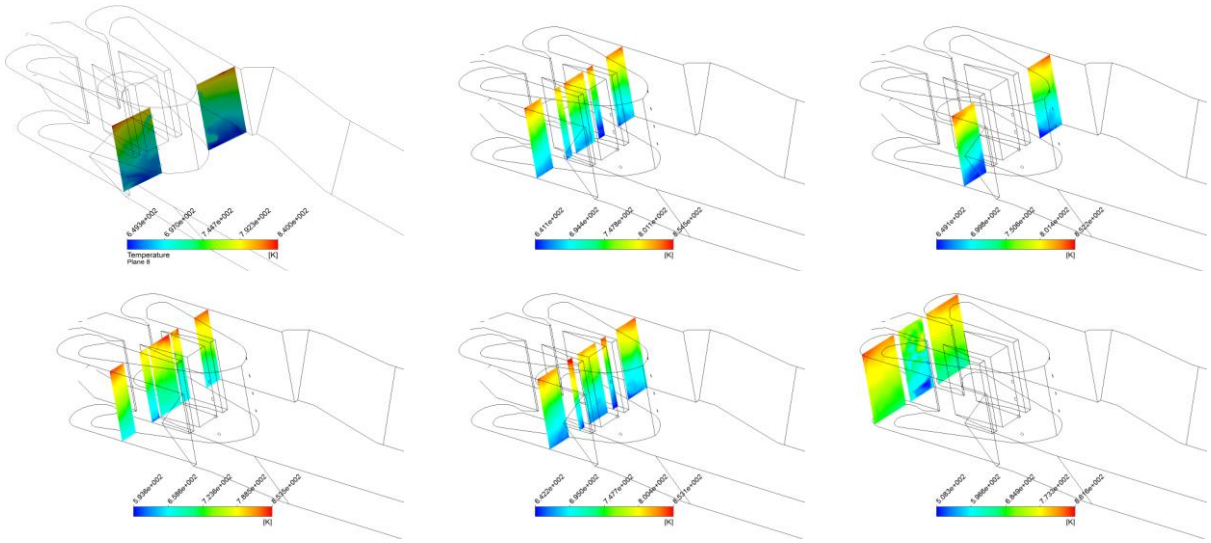

Figure 17 – Temperature distribution at the same axial positions as in Figure 15

This is seen more clearly in the left part of Figure 19 depicting the flow field at the position 3 cm upstream of the fuel inlet. Here a fairly strong flow in the tangential direction against the direction of rotation is present at the centre of the plenum. This will of course also affect the flow in the combustor such that high velocity flow is impinging on the right (or trailing) wall of each of the combustor channels. This is then the cause of the differences in fuel transport seen in Figure 15.

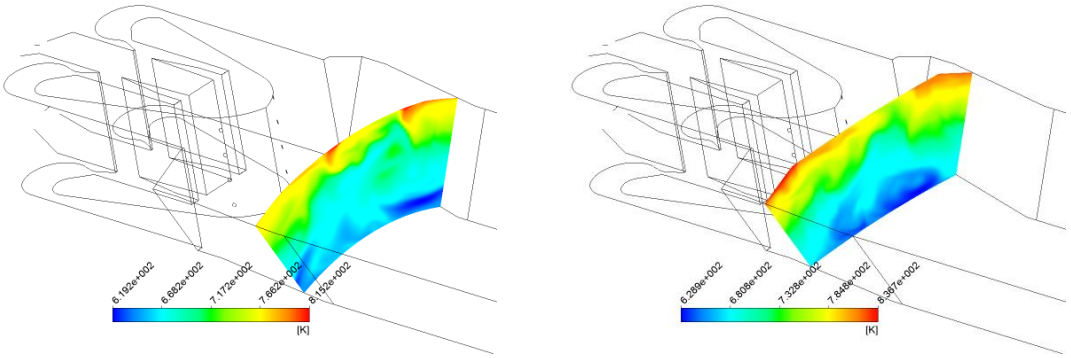

Figure 18 – Temperature distribution at the same axial positions as in Figure 16

To circumvent the issue related to detonation simulation in the full engine, a simplified geometry was developed and the DDTFoam solver in OpenFOAM has been used to simulate detonation both in a 2D and in a 3D domain. The velocity fields for the 3D case are presented in Figure 20.

© TIDE Consortium - *This document and the information contained are TIDE consortium property and shall not be copied or disclosed to any third party without TIDE consortium prior written authorisation*

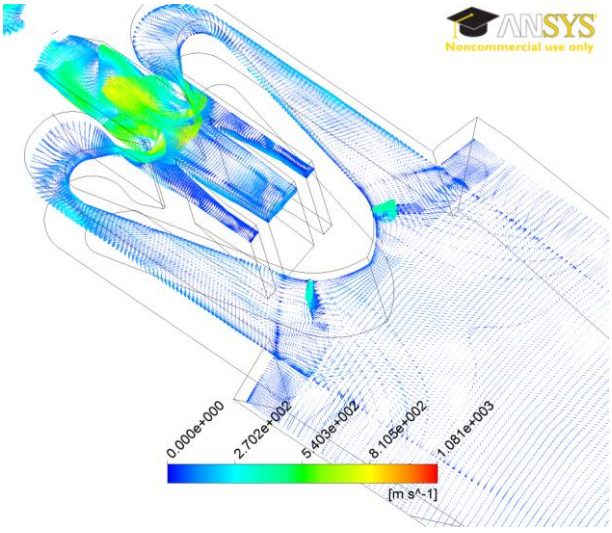

Figure 19 – Flow field in the radial plane through the upper fuel inlets

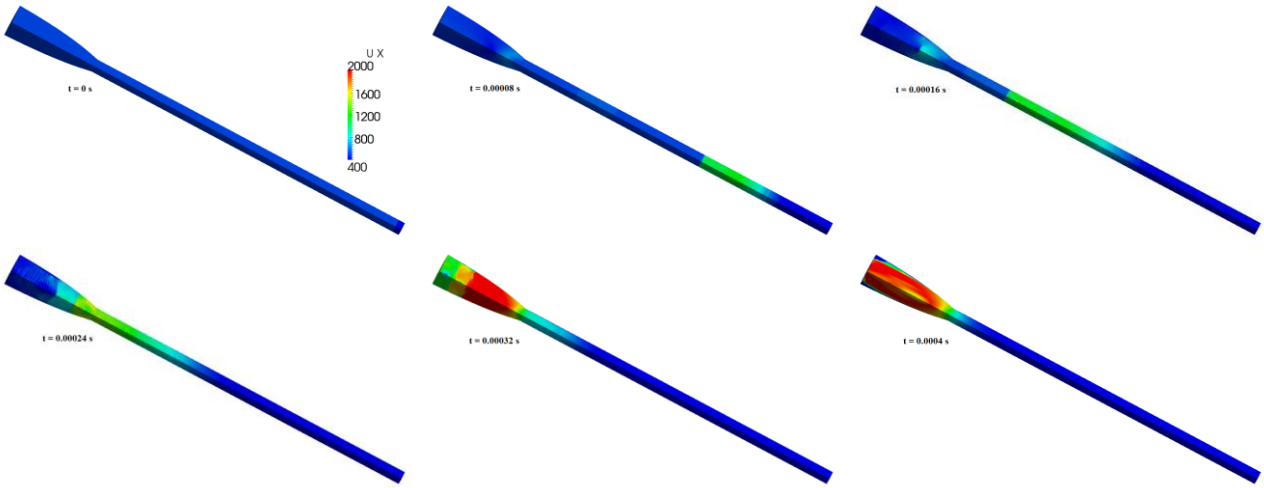

Figure 20 – Axial velocity contours in m/s (3D solution)

In order to evaluate the performance of the engine under detonation, the principal physical quantities are computed at the nozzle exit plane. In particular, a number of points in which the physical quantities are recorded during the simulation have been considered. The mass-averaged quantities are computed considering the values recorded at 10 locations along the radius at the nozzle exit. Figure 21 shows the exit force under detonation for an optimized and for non-optimized 2D nozzle geometry and for 3D nozzle geometry.

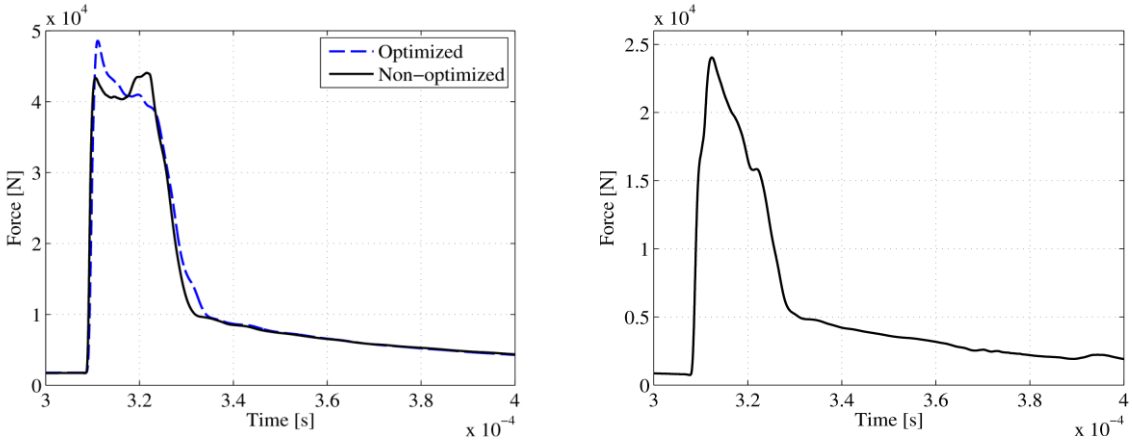

Figure 21 – PDE performance from 2D (left) and 3D (right) simulations

© TIDE Consortium - *This document and the information contained are TIDE consortium property and shall not be copied or disclosed to any third party without TIDE consortium prior written authorisation*

1.3. WP 4 – Geometrical modelling and design

Based on the numerical simulations, the CAD models of the compressor, combustor, and of the full engine were developed and are presented in Figure 22.

For the combustor, assembly and detail drawings were also developed, to serve for the manufacturing of the demonstrator in WP 5. The test rig adaptation required for the experimental program in WP 6 was also carried out in this WP.

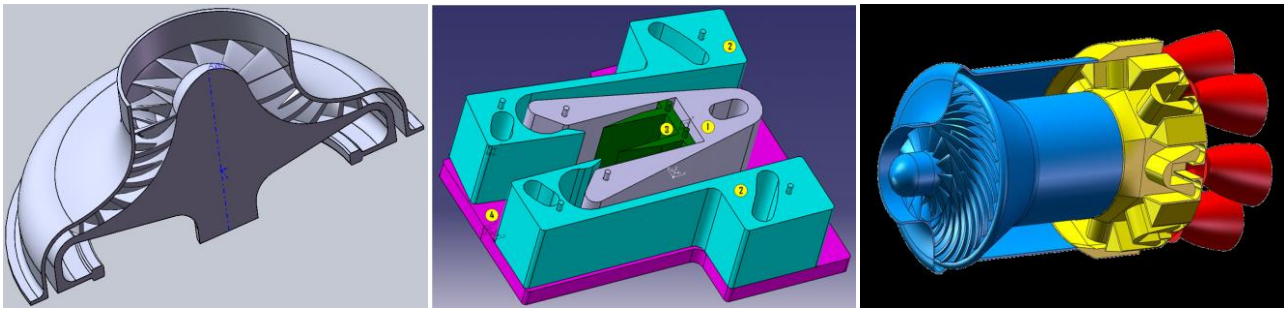

Figure 22 – CAD models for the TIDE compressor (left), combustor (centre) and engine (right)

1.4. WP 5 – Manufacturing and assembly

The most significant achievement of the WP was the manufacturing and assembling of the TIDE demonstrator.

The demonstrator parts have been manufactured and the assembly was made in all the configurations that will be used for the experimental campaign, and presented in Figure 23. There were 54 possible configurations (including the baseline), resulting from:

- Three possible angles of the supersonic jet entering the detonation chamber, resulting from three possible positions of the Semi-casings on the Lateral Walls;
- Three possible distances between the supersonic nozzle and the resonator edges, resulting from the three possible positions of the Detonation Chamber with respect to the Semi Casings;
- Three possible areas of the supersonic nozzle critical section, resulting from three possible positions of the Resonator with respect to the Semi Casings;
- Two possible resonator / main detonation chamber volume ratios, resulting from the two possible resonator geometries.

Besides the manufacturing of the demonstrator, several experimental models for experimentation under non – reactive and detonation conditions were also manufactured. The experimental models used for the detonation measurements in WP 6 are presented in Figure 24.

1.5. WP 6 – Experimental model validation

A first set of significant results were obtained from the experimental study of the interaction of planar supersonic jets and Hartman resonators of various geometries. The dynamics of the oscillating pressure and shock waves system was analyzed in order to define the best suited geometry to serve as basis for the aerodynamic valves that equip the TIDE PDC.

Five types of resonator constructive solutions were experimentally tested, each using several sets of critical geometrical parameters. The tested constructive solutions were:

- V – shaped resonator in open ended channel;
- Two splitters (U – shaped) resonator with open ended channel;
- Two splitters (U – shaped) resonator with closed upstream end;
- Central splitter resonator with closed downstream end;
- U – shaped (two splitters joined by a vertical core)resonator with closed downstream end;
- Single jet step resonator with closed downstream end;

© TIDE Consortium - *This document and the information contained are TIDE consortium property and shall not be copied or disclosed to any third party without TIDE consortium prior written authorisation*

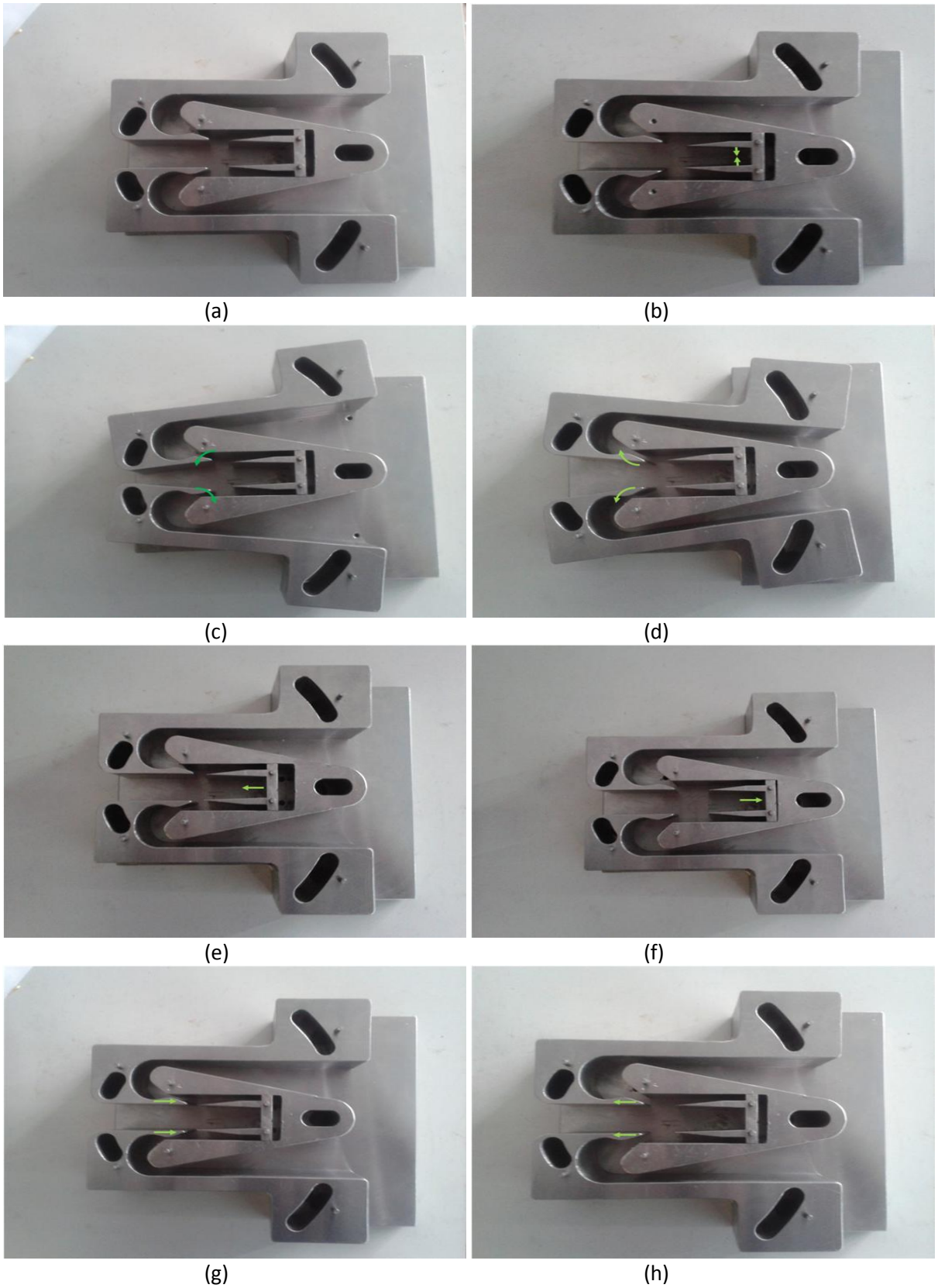

Figure 23 – TIDE demonstrator. a) Baseline; b) Larger resonator / main detonation chamber volume ratio; c) Smaller supersonic jet angles; d) Larger supersonic jet angles; e) Smaller distance between the supersonic nozzle and the resonator edges; f) Larger distance between the supersonic nozzle and the resonator edges; g) Smaller supersonic nozzle critical section area; h) Larger supersonic nozzle critical section area

© TIDE Consortium - *This document and the information contained are TIDE consortium property and shall not be copied or disclosed to any third party without TIDE consortium prior written authorisation*

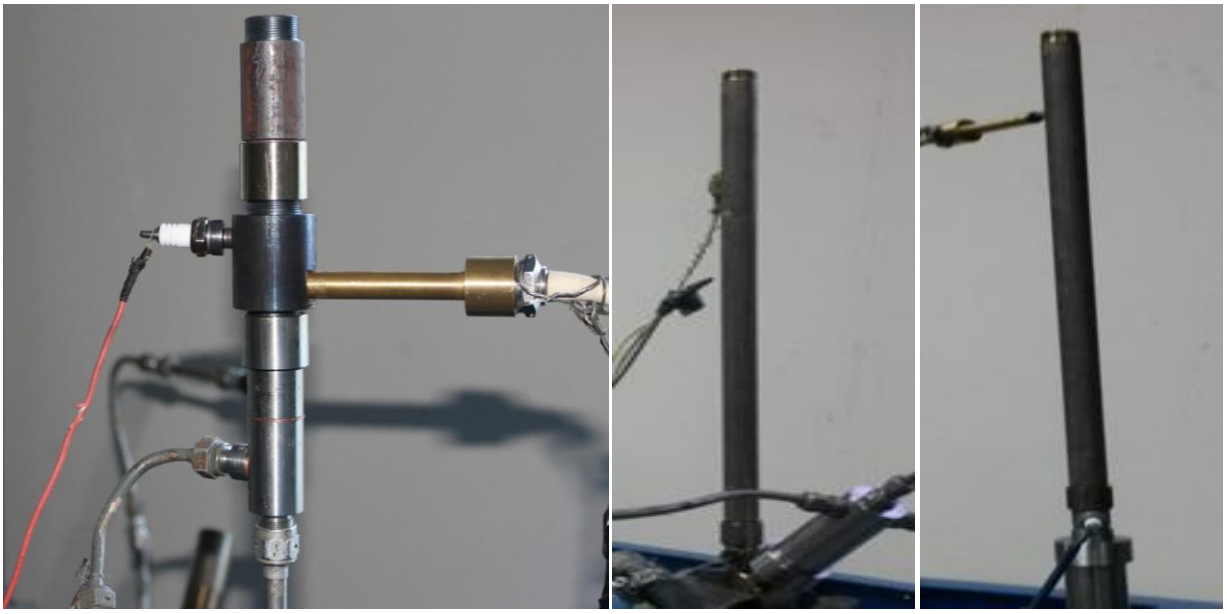

(a) (b) (c)

Figure 24 – Experimental models for detonation measurements. a) Experimental model using the U – shaped resonator; b) Experimental model using the step resonator; c) Experimental model using the dynamics of a planar jet system entering a ring shaped channel

The most significant results were obtained for the U - shaped resonator experimental model with the 60° jet nozzle angle and 12 mm between the jet nozzles and the resonator edges. The configuration was also used for the TIDE demonstrator.

For small angles of the supersonic jets with respect to the demonstrator centreline, the two jets exiting the nozzles turn sharply, reaching over a short distance an almost vertical direction, and merge in the central region of the experimental model into a unique jet. The core of this jet presents small amplitude oscillations both in the horizontal and the vertical direction, producing pressure waves that propagate both upstream and downstream. Pressure oscillations are induced by the two jets in the lateral resonators as well, and the oscillations in them appear to be in phase, and in phase opposition with respect to the pressure oscillations in the central detonation chamber.

As the distance between the jet nozzles and the resonator edges increases, the turning of the jets immediately downstream of the nozzles is less sharp. and the waves propagating inside the lateral resonators are weaker. Vortex propagation downstream of the outgoing supersonic jet is clearly visible. If the distance between the nozzles and the resonator is decreased, the intensity of the unique central jet oscillations is significantly increased, together with the intensity of the vortical structures detaching from the central core and propagating upstream and downstream, both in the central regions, and in the two lateral resonators. The pressure oscillations in the two resonators remain in phase, and in opposition of phase with the pressure oscillations in the central detonation chamber. The vertically propagating pressure waves are stronger than in large distance case.

When the jet angle is increased, the structure of the flow remains similar to the previously analyzed cases, but the amplitude of horizontal and vertical oscillations of the central jet core further increases, generating even stronger vortical structures propagating both upstream and downstream. The synchronization between the pressure oscillations in the resonators is maintained.

Further increasing both the angle and the distance between the resonator edges and the supersonic nozzles leads to a significant decrease in the curvature of the two jets exiting the supersonic nozzles, but otherwise, the pattern of structures remains unchanged, with a pulsating jet core that propagates pressure waves both in the central detonation chamber and in the two lateral resonators and towards the outlet of the experimental model.

© TIDE Consortium - *This document and the information contained are TIDE consortium property and shall not be copied or disclosed to any third party without TIDE consortium prior written authorisation*

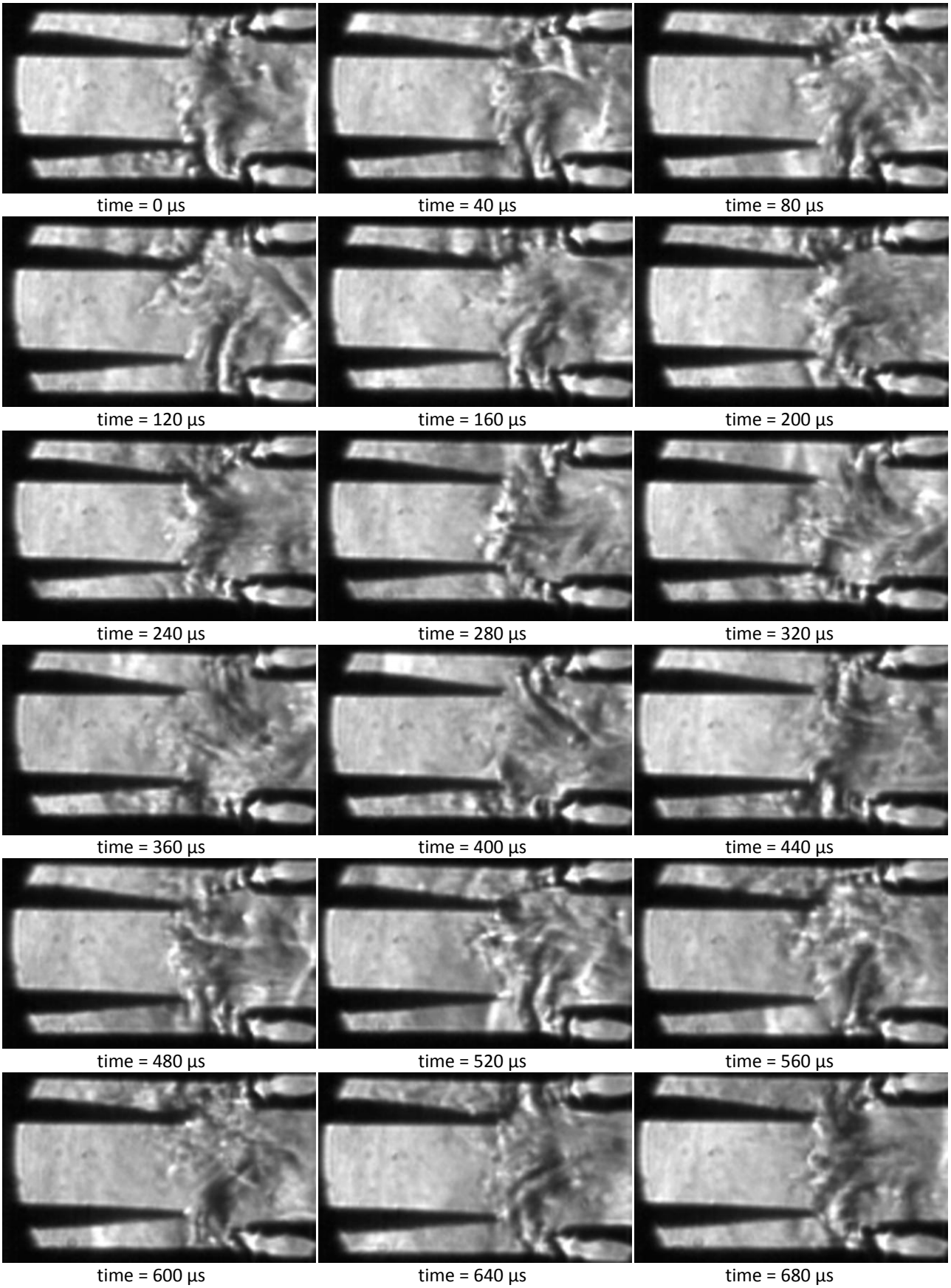

Figure 25– Step –by-step development of the flow structure cycle in the case of the U - shaped resonator experimental model with the 60° nozzle and 12 mm between the jet nozzles and the resonator edges

© TIDE Consortium - *This document and the information contained are TIDE consortium property and shall not be copied or disclosed to any third party without TIDE consortium prior written authorisation*

Reducing the nozzle to resonator distance to 13 mm, the jet core pulsations are significantly reduced, particularly in the horizontal direction. A pair of quasi – stationary shock waves forms at the entrance of the two lateral resonators, anchored on the sharp edges of the resonator, and with the other end oscillating with very small amplitudes along the lateral wall of the experimental model.

These shock waves, anchored around the position corresponding to a normal shock wave, damp the pressure pulsations generated by the supersonic jets and travelling into the lateral resonator. The decrease in the amplitude of the jet core oscillation also reduces the intensity of the pressure waves propagating into the central detonation chamber

Decreasing further the distance from the nozzle to the demonstrator, at 12 mm, a dramatic regime change occurs in the experimental model. The Schlieren images acquired for this case, and presented in Figure 25. The two supersonic jets merge for part of the oscillation cycle into a single jet core in the central region of the experimental model but, contrary to the situation observed for other geometrical configurations, even when the jets are unified in the central region, the resulting continuous structure is weak in the middle. The jets eventually separate and start rotating counter clockwise and away from each other and towards the lateral resonator, where they enter at a certain moment and provide high intensity pressure waves that propagate through them.

These waves reflect on the closed ends of the resonator and return towards the entrance, raising the pressure and forcing the jets to leave the horizontal position and move back towards the centreline, where they merge and form an almost vertical continuous structure. The cycle then repeats. The frequency estimated from Figure 25 is of 1,470 Hz.

A second characteristic frequency is related to the oscillatory rotation of the jets around the nozzle exit section. The frequency of this cycle, as estimated from the Schlieren data, is of 2,080 Hz.

This configuration has, over the open channel solutions, the advantage of focusing the entire jet energy for the creation of the shock waves, without any losses to the atmosphere. In comparison with the central splitter resonator experimental model, the present configuration appears to generate stronger shock waves. Therefore, this solution was preferred for use in the TIDE demonstrator.

If the distance between the nozzles and the resonator edges is reduced again, to 11 mm, the intensity of the pressure waves travelling through the experimental model is larger, due to the higher amplitudes of the jet core pulsations and the flow dynamics resemble the 13 mm case. The amplitudes of the jet core oscillations are significantly more reduced than in the earlier cases, and the shock waves, even if weaker, are anchored at the sharp edges of the resonator. However, in this case, the shock waves do not reach the normal shock wave position, and oscillate slightly along the side wall between oblique shock positions. Their intensity is weak enough that they are not visible in the Schlieren images in certain snapshots. Their reduced intensity allows stronger pressure disturbances to travel through the resonators, and their reflections back to the resonators entrances are not strong enough to trigger a normal shock wave.

Further reducing the distance between the resonator edges and the nozzles, the symmetrical regime is fully recovered the amplitude of the central jet core oscillations and the intensity of the pressure waves travelling through the experimental model increases with decreasing the above distance.

As before, the two supersonic jets merge in the central region and create a unique structure. A central jet core, attached to this structure and oriented outwards is oscillating in both the horizontal and the vertical direction, creating pressure waves that propagate both upstream and downstream.

Besides the constructive solution presented previously, promising results were also obtained for the central splitter resonator and for the single jet step resonator.

The second set of experiments was carried out on the demonstrator developed in the previous WPs and was aimed at understanding the effects of several critical geometrical parameters, as well as of the inlet thermodynamic parameters, on the flow patterns in the demonstrator. The general layout of the pressure and temperature probes is presented in Figure26. The results obtained for the baseline configuration (denoted **0000**) are presented in Figures 27 – 29.

The static pressure decreases strongly through the Laval nozzle, from the upstream position 8, to the downstream position 4, indicating a strong acceleration through the convergent – divergent nozzle section,

© TIDE Consortium - *This document and the information contained are TIDE consortium property and shall not be copied or disclosed to any third party without TIDE consortium prior written authorisation*

characteristic to a supersonic flow. The amplitude of the high frequency oscillations remains the same, of about 20,000 Pa through the nozzle.

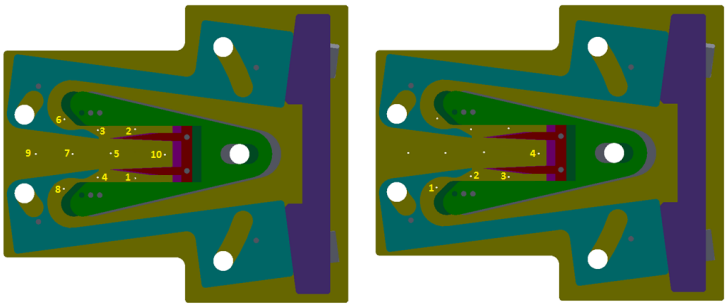

Figure 26 – General layout of the pressure and temperature probes

The low frequency oscillations have lower amplitudes in position 8 (30,000 Pa) than in position 4 (50,000 Pa), as the critical section of the Laval nozzle dampens the oscillations propagating upstream.

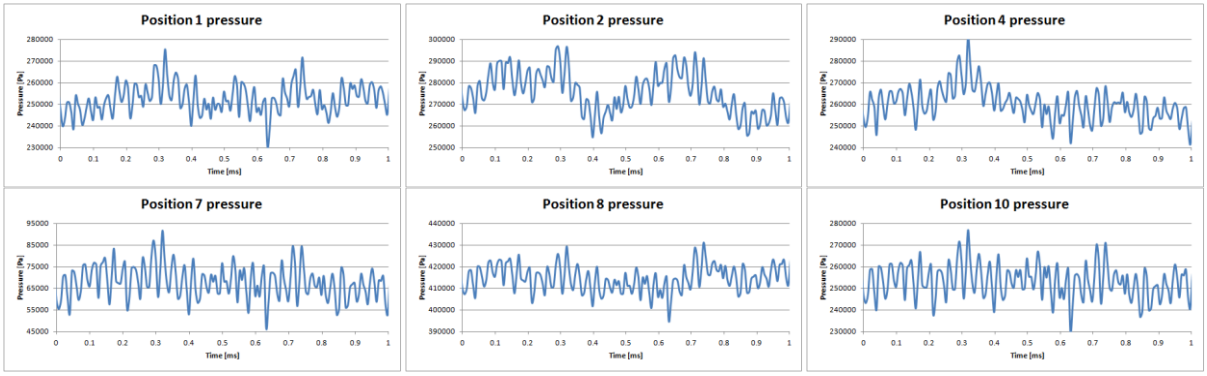

Figure 27 – Pressure signal at in configuration **0000**

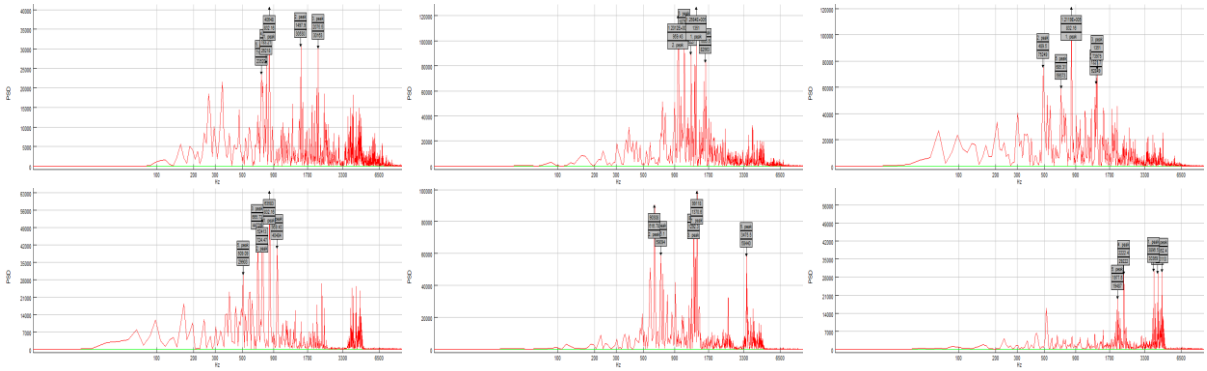

Figure 28 – FFT of the pressure signal in configuration **0000**

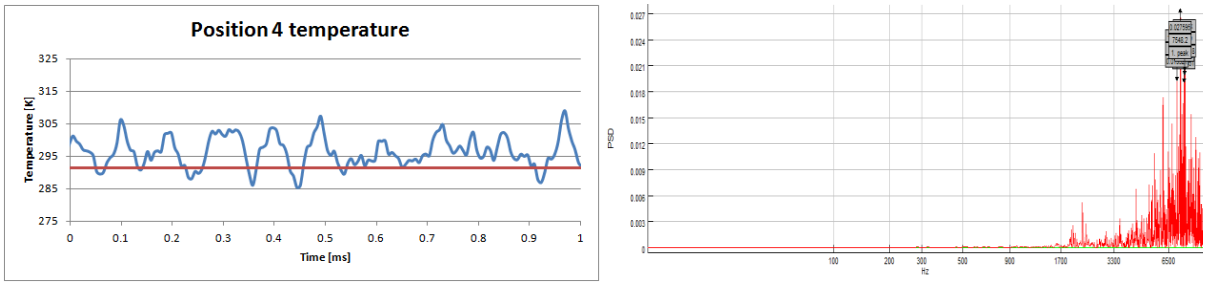

Figure 29 – Temperature signal (left) and its FFT (right) in configuration **0000**. The red line represents the inlet temperature

Further downstream, in the resonator corresponding to the same inlet as for positions 8 and 4, the pressure signal in position 1 indicates slightly lower static pressure values, indicating an increase in velocity

© TIDE Consortium - *This document and the information contained are TIDE consortium property and shall not be copied or disclosed to any third party without TIDE consortium prior written authorisation*

induced in the PDC lateral resonator. The amplitude of the low frequency pressure oscillations remains high, in the range of 50,000 Pa, as pressure waves are propagating from the nozzle exit through the resonator. The frequency of the signal captured by the probe inside the resonator (position 1), presents more dominant frequencies than the signal captured by the probe at the nozzle exit, due to the interference of the waves propagating back and forth through the resonator.

The pressure signal in the opposite resonator, provided by the probe in position 2, is in phase to the pressure signal in position 1, in correlation with the numerical simulations carried out in the same geometrical configuration. In general, the two signals coming from the resonators are similar.

In the central detonation chamber, the pressure signal at position 10 presents significantly lower amplitudes, and is in opposition of phase compared to the signals acquired from the two resonators. The mean pressure value is about the same as inside the resonators.

Further downstream in the central detonation chamber, in position 7, the static pressure mean value decreases substantially, below the atmospheric pressure value, indicating a high velocity in the supersonic jet exiting the PDC. Both the frequency and the amplitude of the pressure oscillations remain similar to those recorded upstream, in position 10.

At the nozzle inlet, in position 8, three dominant frequencies can be observed: the first, in the range 600 – 700 Hz, also observed in the Schlieren data, and related to compressor noise, a second one around 1,300 Hz, and a third at 3,475 Hz. The second frequency, with a highest peak at 1,370 Hz is close to the 1,470 Hz frequency registered for the U - shaped resonator experimental model with the 60° nozzle and 12 mm between the jet nozzles and the resonator edges, which also represents the geometry of configuration **0000**. The high frequency is closer to the typical 4,000 Hz frequency noted in the previous section as typical for planar jet oscillations.

The situation is similar downstream of the nozzle, in position 4, only the high frequency peak now disappears through the effect of the critical section of the nozzle. The low frequency region presents now more clearly separated peaks at slightly lower values (489 Hz, 685 Hz, and 832 Hz), while the middle range frequency remains around 1,300 Hz.

Inside the resonator, along the same streamline as positions 4 and 8, in position 1, the low frequency peaks increase again and shift closer together. The higher frequency is now closer to that observed in the Schlieren data, at 1,498 Hz.

A new frequency peak appears at 2,075 Hz, also observed in the Schlieren data for a similar geometry and related to the oscillatory rotation of the jets around the nozzle exit section. It is interesting that this frequency is only sensed in the resonators, and not in the nozzle measurement position, which is placed upstream of the actual exit and does not capture the jet rotation. The situation is generally similar for the other resonator, in position 2, with a lower frequency for the oscillatory rotation of the jets around the nozzle exit section, around 1,600 Hz, probably due to imperfections of the experimental apparatus.

In the central detonation chamber, in position 10, the low frequency peaks disappear, and the dominant frequencies are now at 1,977 Hz, representing the frequency characteristic to the oscillations of the central jet core, at 2,222 Hz, possibly related to the oscillatory rotations of the supersonic jets, but altered by the interference with the central jet pulsations, and also in the range 3,900 – 4,100 Hz, representing broadband shock noise.

Finally, at the PDC outlet, in position 7, the pressure wave fluctuations are dampened by the straight exhaust channel, and only the low frequency peaks remain, in the region 500 Hz – 1000 Hz, probably related to compressor operation, as noted earlier. A high frequency region, related to shock noise, also exist around 4,000 Hz.

The temperature rise due to shock waves in the PDC is of about 15 K. This is insufficient for Hydrogen self ignition, and it will have to be addressed by either raising the inlet temperature and pressure, or by altering the demonstrator geometry, as discussed in the following sub-section. The temperature signal presents a clearly defined peak at a frequency of 7,548 Hz.

Similar measurements are carried out to evaluate on the dynamics of the flow of the inlet pressure and temperature, of the critical section of the convergent – divergent nozzle, of the angle of the supersonic jets

© TIDE Consortium - *This document and the information contained are TIDE consortium property and shall not be copied or disclosed to any third party without TIDE consortium prior written authorisation*

entering the demonstrator with respect to the centreline, and of the distance between the resonator edges and the outlets of the two supersonic nozzles.

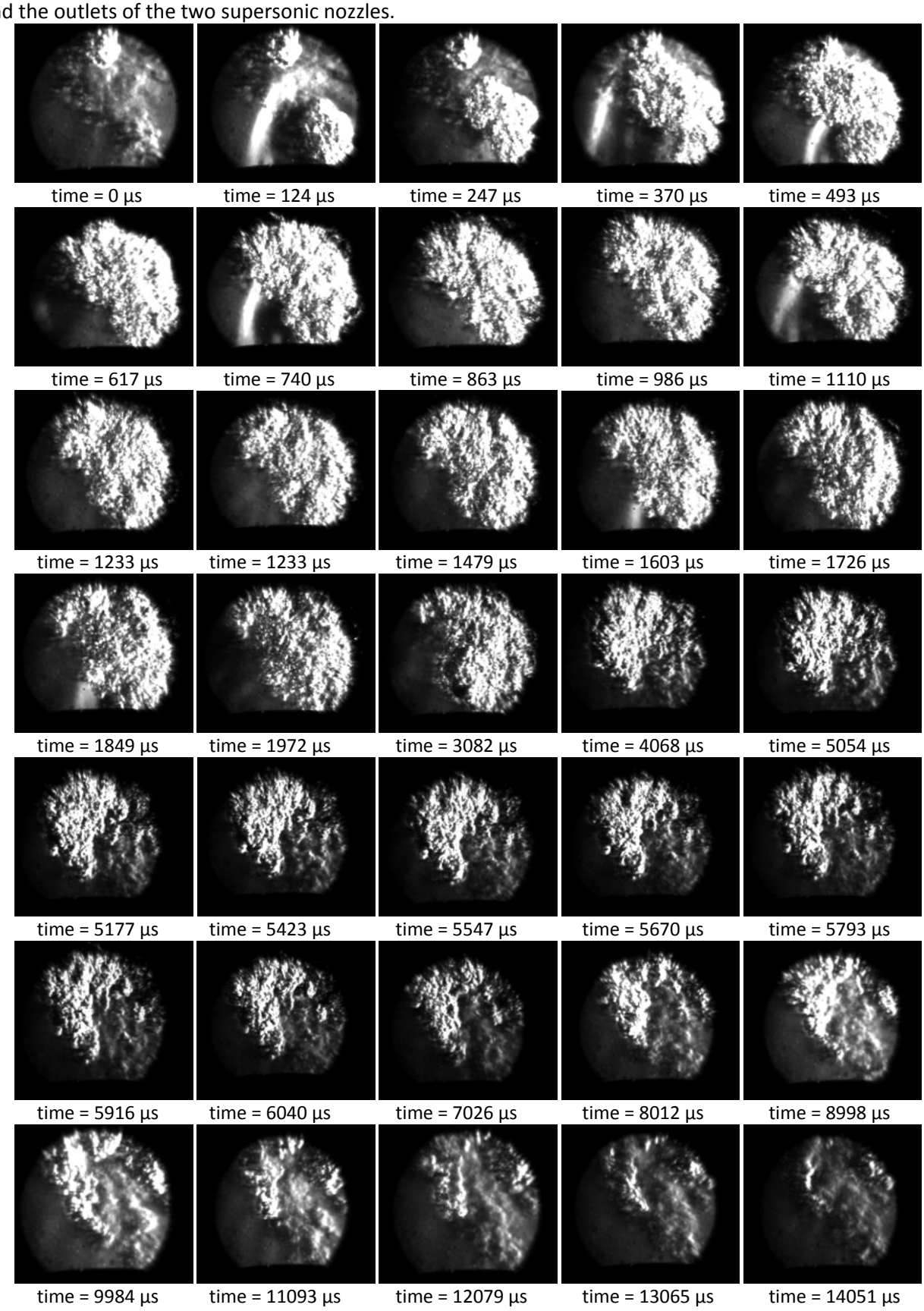

Figure 30 – Development of detonation process in the U – shaped resonator experimental model

© TIDE Consortium - *This document and the information contained are TIDE consortium property and shall not be copied or disclosed to any third party without TIDE consortium prior written authorisation*

It is found that the critical geometrical parameters are the last two, and that the increase in temperature tends to increase the temperature rise through the shock waves.

Finally, a set of three experimental models were tested under detonating condition to provide proof of the TIDE concept.

Figure 30 presents the Schlieren visualizations of the flow through the experimental model based on the U – shaped resonator, the same that was used for the TIDE demonstrator.

Detonation was achieved in the demonstrator for an inlet pressure of 7 bars. A spark plug was used to ignite the Hydrogen – air mixture immediately downstream of the resonator. The data is acquired downstream of the resonator and of the spark plug.

The cycle starts with a clearly defined shock wave travelling immediately upstream of the combustion wave (time 124 μs), and forming together the detonation wave. The achievement of detonation in the experimental model represents the required proof of concept that was the main objective of the TIDE project. The fulfilment of this main objective is, hence, demonstrated here.

It is also very important to note that the process is cyclic, with a stable frequency of about 70 Hz, indicating the proper operation of the aerodynamic valves built into the system. This demonstrates the achievement of another major goal set forth at the beginning of the TIDE project. As the combustion products following the detonation wave enter the visualization channel, of significantly larger cross – section, expansion waves are formed (time 370 μs) and the velocity of the burned gas jet decreases. The shock wave continues to move outwards, following a spherical propagation pattern at a high velocity estimated from the Schlieren data at the Chapman – Jouguet velocity, and decouples from the burned gas jet front.

Next, as the jet of combustion products develops in the visualization chamber, moving upstream and spreading, a series of increasingly weaker shock waves propagate from the resonator into the visualization chamber (time 370 μs, time 493 μs, time 740 μs, time 986 μs, time 1603 μs, time 1849 μs). The frequency of the occurrence of these waves appears also to be diminishing in time. The reason behind their formation and propagation might be related to the operation of the resonator under detonation conditions, but further investigations are required using a higher temporal resolution of the high speed camera, and, ideally, optical access into the region where the resonator is placed in order to fully understand the phenomenon.

The ignition does not reoccur for a relatively long period of time, the next detonation wave (not captured in the images presented in Figure 30) entering the visualisation chamber at a time between 14051 μs and 14297 μs. This correlates with the spark plug operating frequency, of 70 Hz, indicating that the detonation cycle installed in the experimental model is not self – sustained, ignition occurring only when triggered by the spark plug. This is a shortcoming of the model that will need to be addressed. Efforts to overcome the issue were made within the project, and the results will be presented in the following, but further research will be undoubtedly needed.

The shape of the pressure wave collected inside the experimental model is presented in Figure 31.

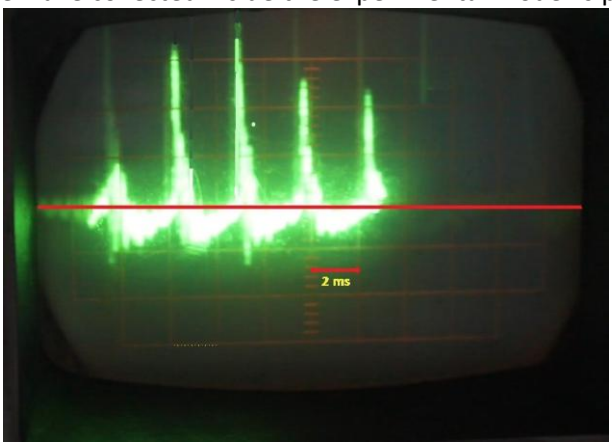

Figure 31 – Pressure signal from the experimental model based on the U – shaped resonator

© TIDE Consortium - *This document and the information contained are TIDE consortium property and shall not be copied or disclosed to any third party without TIDE consortium prior written authorisation*

A second experimental model based on the single jet step resonator was also tested under detonation conditions is. The shape of the pressure wave captured in this experimental model is characteristic for detonation. The signal, however, is irregular, both in amplitude and in frequency. The problem occurs when the detonation is not self sustained and is initiated only by the sudden energy release of a spark plug. In this case, the detonations process is driven by the spark plug frequency, which does not, normally, correspond exactly with the natural frequency of the resonators. The mismatch leads to frequency shifts in the PDC operation, irregular detonation wave amplitudes, and even to misfires.

Concluding, the experiments have shown that the step resonator is a viable solution, providing a functional experimental model able to achieve the strong aerodynamic pulsations needed for PDC operation, but the issue of achieving self – sustained detonation remains open, as in the case of the previous model.

In an effort to solve the remaining issues observed in the previously presented model, a new solution was developed and tested experimentally. The solution is based on the dynamics of a planar jet injected into a circular sing shaped channel. Previous research studies indicate that the injected jet creates an oscillating torsion motion in the ring shaped channel, with a periodical displacement from the symmetry axis. The same phenomenon was demonstrated to occur in systems of planar jets, and the research carried out within the present project shows that the phenomenon remains qualitatively similar for supersonic jets.

Here, several planar supersonic jets enter a circular ring shaped channel delimited by a diaphragm. The fuel jet is also brought in the same channel, where mixes with the air through the interaction between the air jets and the fuel jet.

The perfection of the mixing process is critical to achieve detonation, as it will be demonstrated in the following. Therefore the mixing enhancement by supersonic jet oscillations is one of the key elements of the optimal solution.

The pressure signal captured from within the experimental model shows the characteristic shape of the detonation wave. The amplitude of the pressure oscillation resulting from the detonation is very high, indicating a strong detonation wave and a satisfactory operation of the experimental model, made possible by the use of the premixer based on planar jet oscillations in a circular ring – shaped channel.

The pressure signals are seen to be quite regular, both in amplitude and in frequency, indicating a good detonation control, and a good operation of the experimental model. The amplitude of the pressure signals is larger than in the previous cases, but the frequency of the detonation cycles is lower than in the step resonator case.

The Fourier transform of the detonation pressure signal indicates a characteristic frequency of 100 Hz, which is also the operation frequency of the spark plug. This shows that the detonation is still not self – sustained and is triggered only by the energy released by the spark plug, and not by the conditions created in the detonation chamber.

The issue must be addressed by future research studies. At this point, it is believed, based on the experience gained in the project, that self sustained ignition should be possible if the inlet air stream is preheated at the value expected at the outlet of the TIDE compressor. A further enhancement of the shock waves intensity that can be expected in the demonstrator due to the larger detonation chamber volume, higher mass flow rates, and lower heat and friction losses at the walls should also support self sustained ignition.

A higher spark plug frequency, not allowing the cooling of the gas stream inside the detonation chamber between two forced ignitions may also allow the disconnection of the spark plug after the first few warm – up cycles.

A second significant broadband frequency peak is visible at around 2,050 Hz and characterizes the shock wave generation by the oscillation of the two planar supersonic jets.

© TIDE Consortium - *This document and the information contained are TIDE consortium property and shall not be copied or disclosed to any third party without TIDE consortium prior written authorisation*